Natural Resources Canada | Ressources naturelles Canada

GEOLOGICAL SURVEY OF CANADA
OPEN FILE 7881

# Geophysical, geotechnical, geochemical, and mineralogical data sets collected in Champlain Sea sediments in the Municipality of Pontiac, Quebec

**H. Crow, S. Alpay, M.J. Hinton, R.D. Knight,
G.A. Oldenborger, J.B. Percival, A.J.-M. Pugin, and P. Pelchat**

**2017**


**GEOLOGICAL SURVEY OF CANADA**
**OPEN FILE 7881**

# Geophysical, geotechnical, geochemical, and mineralogical data sets collected in Champlain Sea sediments in the Municipality of Pontiac, Quebec

**H. Crow, S. Alpay, M.J. Hinton, R.D. Knight,**
**G.A. Oldenborger, J.B. Percival, A.J.-M. Pugin, and P. Pelchat**

**2017**



doi:10.4095/301664

This publication is available for free download through GEOSCAN (http://geoscan.nrcan.gc.ca/).

**Recommended citation**
Crow, H., Alpay, S., Hinton, M.J., Knight, R.D., Oldenborger, G.A., Percival, J.B., Pugin, A.J.-M., and Pelchat, P., 2017. Geophysical, geotechnical, geochemical, and mineralogical data sets collected in Champlain Sea sediments in the Municipality of Pontiac, Quebec; Geological Survey of Canada, Open File 7881, 1 .zip file. doi:10.4095/301664

Publications in this series have not been edited; they are released as submitted by the author.

# Contents

# Appendices

Digital Appendix A – Field work

- A-1 Microtremor Results
- A-2 Seismic Reflection Profiling
- A-3 Downhole geophysical logging
- A-4 Electrical Resistivity Imaging

Digital Appendix B – Laboratory Work

- B-1 Core logs and photographs
- B-2 Mineralogy report
- B-3 pXRF data

## 1.0 Introduction

In 2010, the Geological Survey of Canada (GSC) began conducting geophysical investigations in western Quebec on Smith-Leonard Road in the municipality of Pontiac (Figure 1). The study area is situated in and around Breckenridge Creek Valley where numerous landslides, both ancient and modern, have been identified in the silty-clayey Champlain Sea sediments of the region (e.g. Eden and Mitchell, 1970; Mitchell, 1970, Brooks et al, 2013). Four of these landslides in the study area have the age signature of a paleoseismic event 1020 years before present (yr BP) (Brooks et al., 2013), indicating that these soils are susceptible to earthquake-triggered ground failure. Additionally, the low shear wave velocities of these soft sediments which overlie high velocity bedrock create conditions leading to significant amplification of earthquake shaking (e.g. Kramer, 1996; Hunter et al., 2010; Crow et al., 2011; Khaheshi Banab et al., 2012). Therefore, GSC studies were undertaken at the site through the Public Safety Geoscience Program to investigate the geophysical, geotechnical, and geochemical properties of the sediments, and the shape of the bedrock basin underlying them. The purpose of the multidisciplinary approach was to gain a better understanding of how these materials might respond to earthquake shaking, allowing for the development of a well-studied test site where future earthquake monitoring could be conducted.

Geophysical techniques employed on site included microtremor recordings, high-resolution seismic profiling, electrical resistivity imaging, and downhole geophysical logging to assess the vertical and lateral variability of sediment properties *in situ*, and investigate the trends of the bedrock surface. Undisturbed core samples (76 and 152 mm diameter) collected in three co-located boreholes were tested in GSC labs to assess geotechnical and mineralogical properties of the sediments, and to test the geochemistry of the pore waters extracted from the soil samples. Some of these samples were integrated into a collaborative GSC research project with Laval, Carleton, and Waterloo universities to study soil response in the lab to increasing levels of strain (Duguay-Blanchette, 2016).

This open file documents the field and laboratory work conducted by the GSC between 2010 and 2017 at Breckenridge Creek, QC, and presents the resulting GSC data sets from these investigations.

### 1.1 Site selection and GSC work in Breckenridge Creek area

Early observations of landslides in the Pontiac area are described in a GSC memoir by Wilson (1924). The National Research Council of Canada undertook studies within Breckenridge Creek in the 1960's following a retrogressive flow slide (23,000 $m^3$) in 1963 (Crawford and Eden, 1967; Mitchell, 1970; Eden and Mitchell, 1970). In the mid 1990's and again in the early 2010's, the GSC worked in the Breckenridge Creek Valley to collect and date organic material relevant to the age of numerous landslides. Four of these dated landslides are part of a larger set of commonly aged landslides that are interpreted to be the product of a paleoearthquake (~$M_w$6.1), occurring at ~1020 calibrated radiocarbon years BP (Brooks, 2013; Brooks et al., 2013).

Strong shaking during small to moderate modern-day earthquakes has been reported by local residents living on the soft Champlain Sea sediments in the Pontiac region. During the June 23, 2010 Val-des-Bois $M_w$5.0 earthquake, located 55 km NE of the site, landowners at the test site reported effects of Mercalli intensity VI to VII (strong to very strong). Site effects ranged from heavily swaying hydro poles and farm equipment, to roaring sounds and waves travelling in directions opposite to the earthquake epicenter. An exterior structure (barn with cement foundations) suffered moderate damage at its base. Shaking intensity reports submitted to the Earthquakes Canada website following this earthquake from across the region are presented in Halchuk (2010).

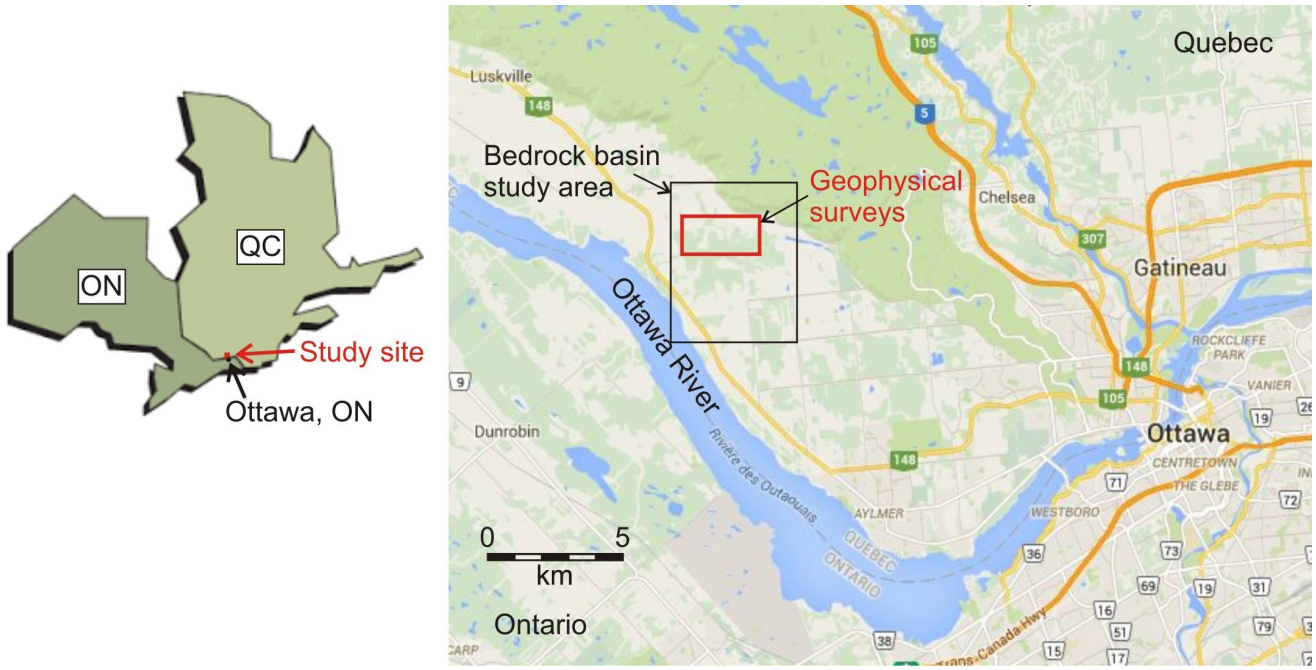


**Figure 1**. Breckenridge Creek study area northwest of Ottawa, ON, in the municipality of Pontiac, QC. The larger rectangle indicates the limits of the bedrock basin investigation; the smaller region within indicates where the geophysical surveys were focused, in the center of the basin. © Google Maps 2016.

GSC experience in this area led to the selection of a test site on a rural property along Smith-Leonard Road, Pontiac, Québec, located along a tributary to Breckenridge Creek (Tributary "A", Figure 2). Records from an existing borehole database identified a buried bedrock basin filled with soft sediments which underlay the site (Bélanger, 2008). In 2010, the first geophysical surveys were carried out, including:

- 3.2 km of 144-channel high-resolution seismic reflection profiling to investigate the P- and S-wave velocity of the sediments, the topography of the bedrock surface, the sedimentary structure of the Champlain Sea sediments beneath the profiles, and the degree of sediment disturbance in an area affected by frequent landslides; and
- 60 fundamental site period measurements to estimate the shape of the bedrock basin in the area surrounding the seismic measurements.

Based on the results of this work, drilling and additional geophysical surveys were undertaken to better understand the physical and geotechnical properties of these sediments (see Figure 2), including:

- drilling and sampling of three boreholes (BH-GSC-BRK-01, -02, -03) situated near the deepest part of the basin in soils undisturbed by mass movements (2010-2014);
- an additional 112 fundamental site measurements to better define the shape of the bedrock basin (2014);
- borehole geophysical logging within the deepest borehole (75 m) using natural and active gamma, induction (apparent conductivity and magnetic susceptibility), and downhole S-wave techniques (2014); and
- 1.7 km of electrical resistivity profiling passing by the boreholes to identify changes in the trends of soil conductivity in the soft sediments (2014).

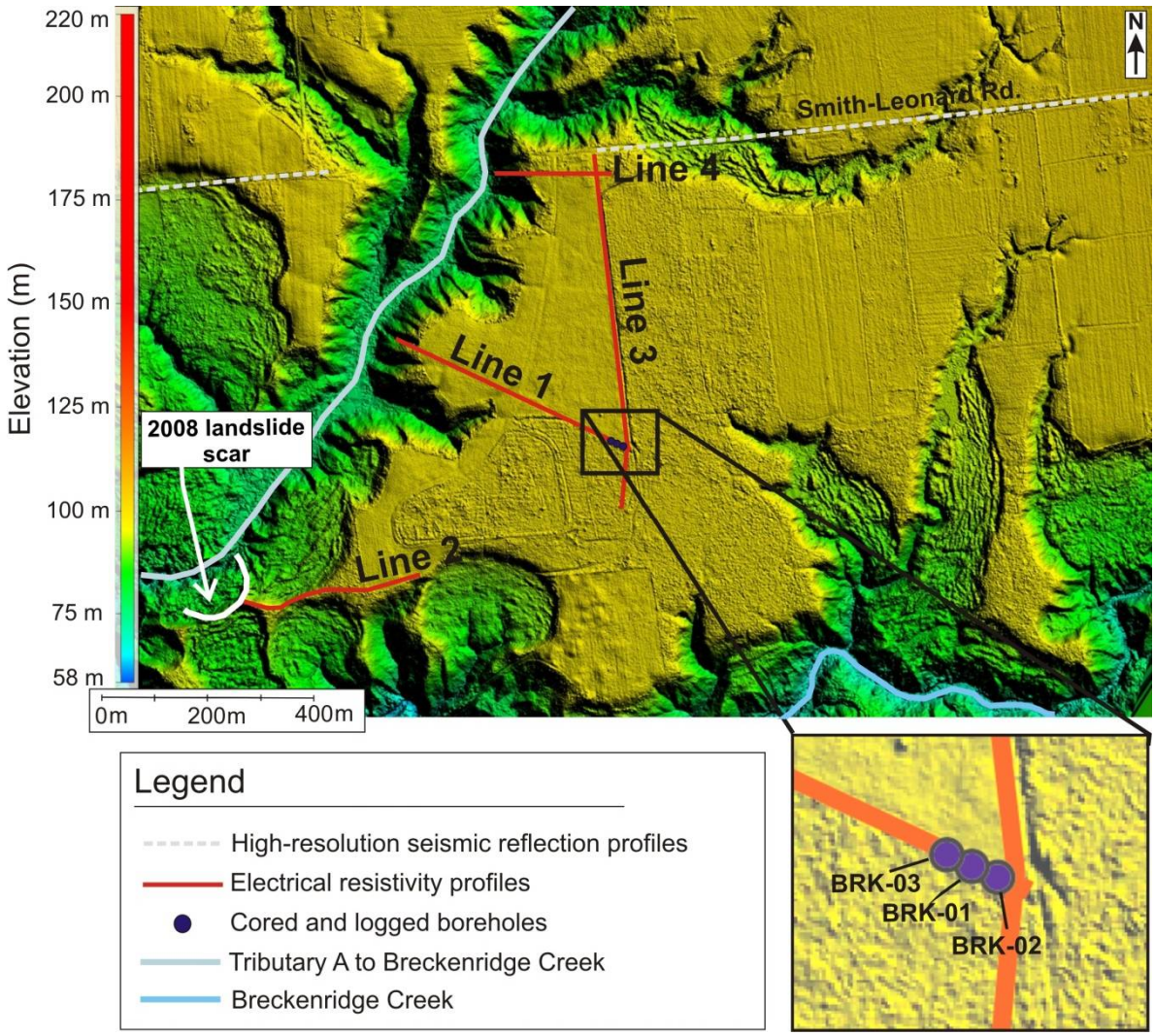


**Figure 2**. Locations of seismic reflection, electrical resistivity imaging, and downhole geophysical logging surveys within the Breckenridge study area. Profiles are shown over a LiDAR image to highlight the prevalence of landslides in the area.

## 2.0 Field work

### 2.1 Microtremor recordings for resonator mapping

In areas where soft soils overlie competent materials (rock or till), vertically traveling weak motion earthquake energy can resonate with very high amplitudes. The frequency (or period) of this resonance is governed by the average shear wave velocity of the soft soil and the thickness of the layer. Nakamura (1989) introduced a method to estimate the fundamental site period, $T_0$, or site frequency, $f_0$ (equivalent to $1/T_0$) using ambient seismic noise in the same frequency range as earthquake energy. The horizontal-to-vertical spectral ratio (HVSR) of this recorded noise can indicate a peak frequency equivalent to the resonant frequency of the site. Following on Nakamura's work, a project named "**S**ite **E**ffect**s** Assessment Using **Am**bient **E**xcitations" (SESAME) was undertaken between 2001 and 2004 by 14 European research institutes which studied the ambient noise technique in detail. The guidelines for best practices using this technique have been published (SESAME, 2004) and are now considered standards for the method.

A microseismograph instrument specifically designed for HVSR measurements called a Tromino (manufactured by MoHo s.r.l. in Italy) was used to collect $T_o$ at 172 sites within the Breckenridge study area. UTM co-ordinates at these sites, and an additional 24 bedrock outcrops (where $T_o$=0), were collected with a handheld GPS (McPeak, 2015). Table 1 describes the data collection and processing parameters for the ambient noise recordings. The processing was carried out using Grilla software designed for the Tromino unit, which incorporates the SESAME testing criteria. The resulting frequencies and periods, as well as the acceptance parameters at each test site are presented in Appendix A-1. Examples of processed microtremor data from the Ottawa area on Champlain Sea sediments are provided in Hunter et al. (2010).

**Table 1.** Data collection and processing parameters for ambient noise measurements using a Tromino seismograph.

| | |
|---|---|
| 3-component sampling rate | 128 samples/second |
| Orientation of sensors | approximately N-S, E-W |
| Recording Time | 30 minutes |
| Processing window | 60 seconds |
| Spectral Filtering | Konno-Omachi Algorithm b = 40 |
| Editing | Manual selection of windows with arithmetic averaging |
| Spectral Windows | 0.1 Hz to 20 Hz |

To relate a fundamental site frequency ($f_o$) to a resonating layer depth, an equation [1] was developed specifically for Champlain Sea sediments in the Ottawa-Gatineau area (Figure 3). The relationship is based on recordings at 98 sites, where a microtremor recording was co-located with a 24-channel seismic reflection/refraction survey. At each site, depth to resonator (or impedance contrast) was computed based on a shear wave velocity analysis (see Hunter et al., 2010). A best-fit power law equation was determined:

$$Z = 60.38 f_o^{-1.158} \pm 17.66\, m\ (2\sigma) \qquad [1]$$

where Z is depth in metres and $f_o$ is fundamental site frequency ($1/T_o$) in Hz.

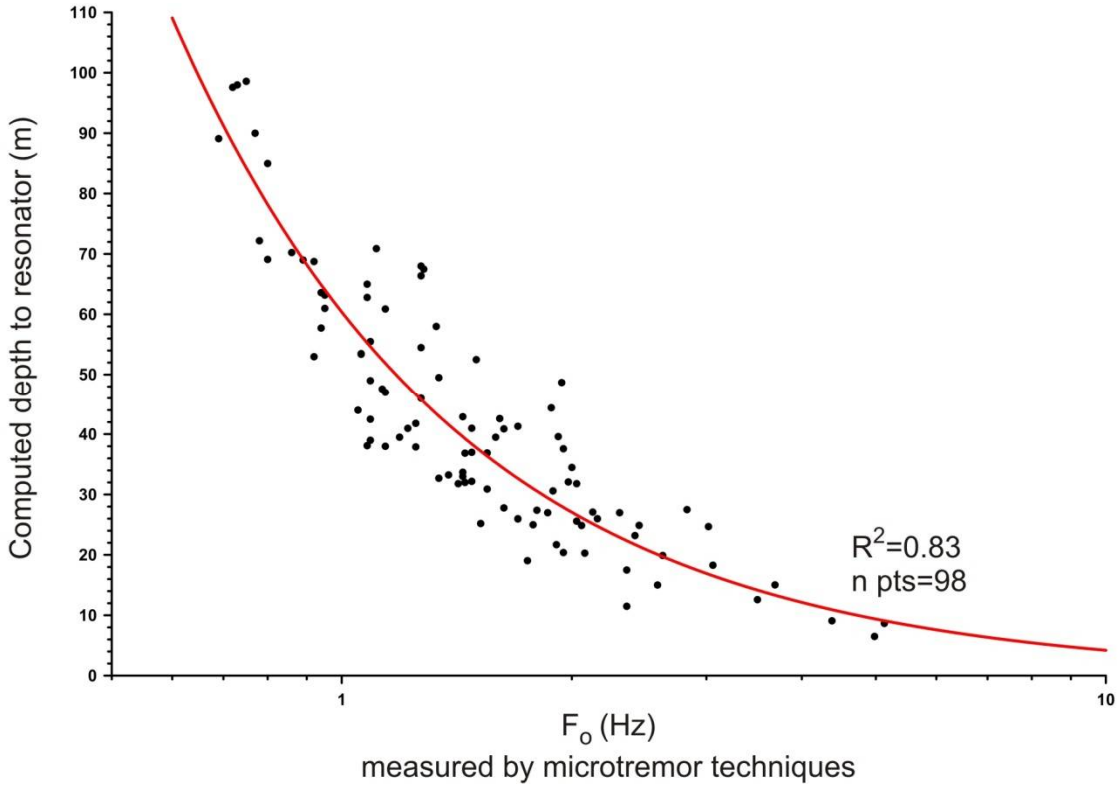


**Figure 3.** Plot relating fundamental site period ($F_o$) to depth calculated at 98 seismic reflection/refraction test sites on Champlain Sea sediments in the Ottawa-Gatineau area.

At each of the 172 HVSR sites, an elevation in metres above sea level (masl) was extracted from a LiDAR map of the area released by the Gouvernement du Québec (2016). By subtracting the soil thickness (Z) from elevation, a resonator elevation was computed. A contour map showing the location of the measurements and the interpreted resonator (till or bedrock) topography is shown in Figure 4. The data reveal an oblong basin, approximately 5 km along axis and 3 km wide, with soft sediment thicknesses reaches up to 98 m. The basin runs parallel to the edge of the Eardley Escarpment which forms a prominent bedrock ridge in the region.

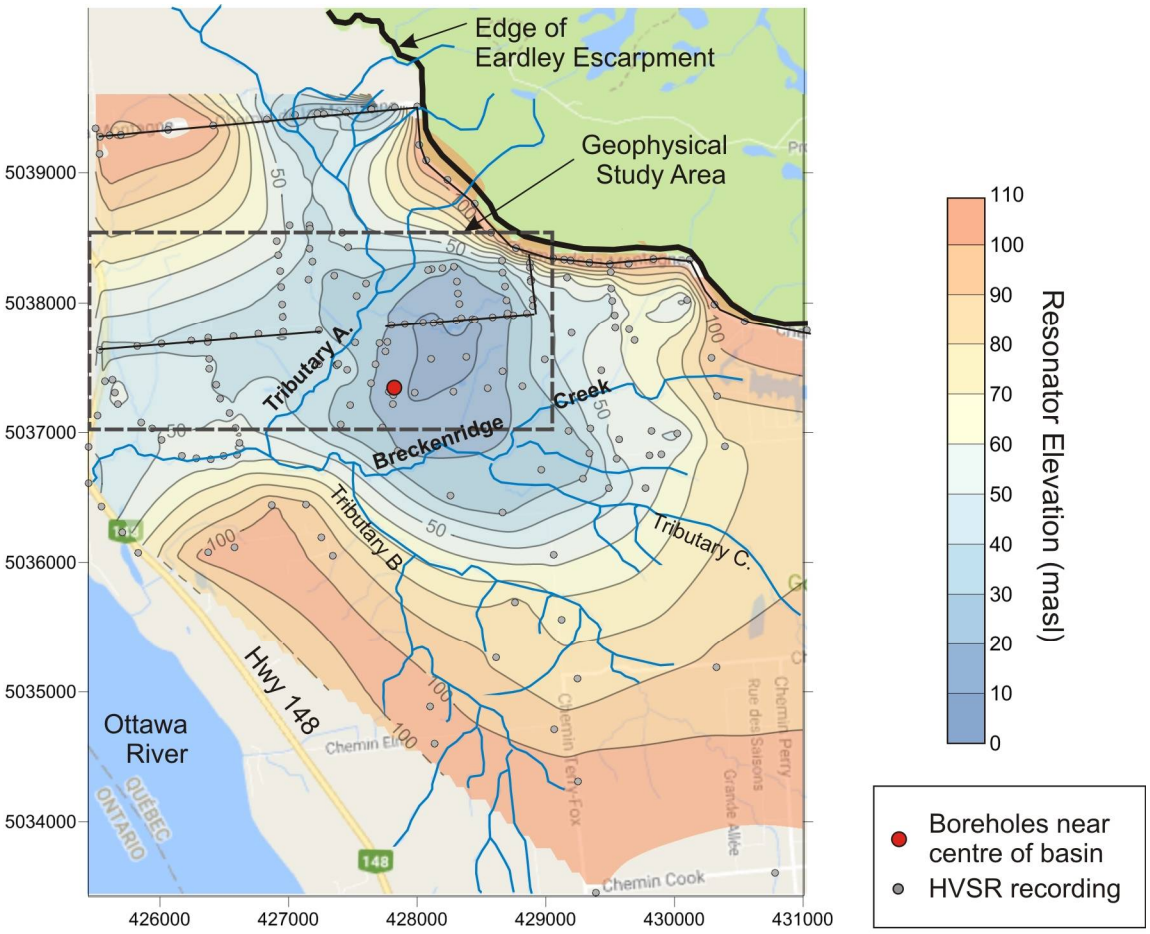


**Figure 4.** Contour map showing the resonator elevation (till or bedrock) in metres above sea level. A deep oval-shaped basin is visible underneath the geophysical study area, where soft sediment thickness reaches 98 m. The upper edge of the grid is defined by the outcropping bedrock of the Eardley Escarpment. © Google Maps 2017.

## 2.2 High resolution seismic profiling

As part of the geophysical studies in the area, the GSC collected 3.2 line-km of high resolution seismic reflection data along Smith Leonard and Townline Rds. The profiles were collected in three segments on either side of Tributary A (to Breckenridge Creek) which splits the road in two (Figure 5). The goal of the profiling was to interpret depth to bedrock beneath the profiles, calculate shear wave velocities of the soft sediments and till overlying the bedrock, and investigate the structure within the disturbed and undisturbed glaciomarine sediments found underneath the roadway.

For high-resolution shallow seismic surveys, the GSC developed a vibratory source-landstreamer data acquisition system which greatly improves the efficiency with which shallow seismic reflection data can be collected, and allows both compressional (P-) and shear (S-) wave data to be obtained simultaneously (Pugin et al., 2009a,b, Pugin et al., 2013a,b,c). For the Breckenridge surveys, the GSC used a three-component (3-C) landstreamer receiver array coupled with a vibrating seismic source (Figure 6). Work was carried out along

Smith Leonard and Townline Rds. (gravel surface) with a crew of 4 people on May 20th and 21st, 2010. Co-ordinates of the start and end positions of the profiles are listed in Table 2.

The seismic source was an IVI (Industrial Vehicles International, Inc) "Minivib" vibratory mass mounted on a "minibuggy". The 140 kg mass (Figure 5b) can be vibrated in either vertical or horizontal mode, and the operator can program a sweep of frequencies through a range between 10 and 550 Hz. For the Breckenridge surveys, the Minivib was operated in the inline horizontal vibrating mode ("H1") using a 7 second linear sweep from 20-350 Hz. The Minivib is equipped with a Trimble DSM 232 with Omnistar differential GPS for positioning, and a high-precision distance-measuring odometer linked to a small readout screen mounted in the cab, allowing the operator to move accurately to the next shotpoint. Data were recorded using six 24-channel Geometrics Geode engineering seismographs operated in the cab of the Minivib. Uncorrelated records are recorded to allow for pre-whitening of the data during processing.

The GSC landstreamer array is designed for use along paved or gravel roads, and is built with 3 kg metal sleds connected using wire or low-stretch belts. For the Breckenridge surveys, the landstreamer array consisted of 48 sleds spaced 0.75 m apart. Each sled was equipped with a 3-component (3-C) geophone unit constructed in-house with 30 Hz omni-directional geophone elements oriented in three directions: one vertical and two horizontal, in-line and cross-line. Three-component data were acquired with shotpoints every 3.0 m along the survey lines.

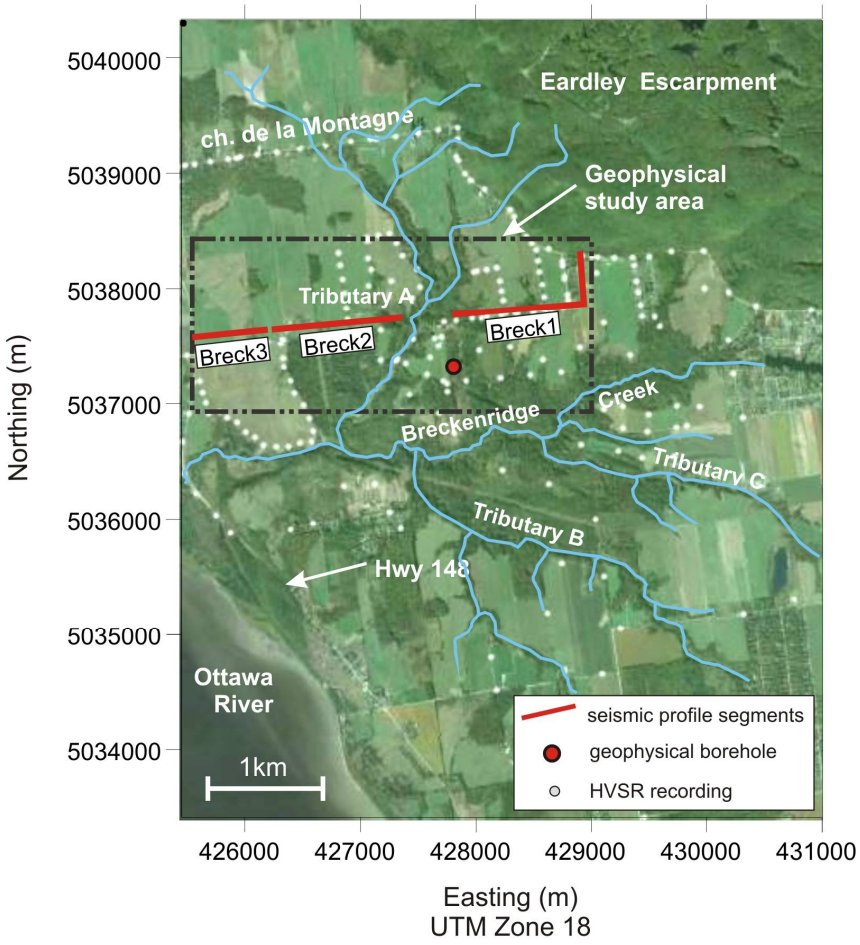


**Figure 5.** Locations of seismic profiles along Smith Leonard and Townline Rds. © Google Maps 2016

**Table 2.** UTM co-ordinates (Zone 18) for start and end positions of the seismic lines along Smith Leonard Rd. East and West refer to either side of the creek dividing Smith Leonard Rd.

| Profile | Easting Start | Northing Start | Easting End | Northing End | Length (km) |
|---|---|---|---|---|---|
| Breck 1 - East | 428868 | 5038318 | 427657 | 5037811 | 1.6 |
| Breck 2 – West-central | 427222 | 5037781 | 426214 | 5037698 | 1.0 |
| Breck 3 – West | 426209 | 5037698 | 425652 | 5037636 | 0.6 |


**Figure 6.** (a) Minivib "minibuggy" seismic source towing a landstreamer array along Smith-Leonard Rd. (b) the Minivib's vibratory source. (c) the Minivib equipped to tow 48 3-component sleds down the gravel roadway.

The steps followed to process the shear wave data are outlined in Table 3. The resulting profiles in time scale, and the interval and average velocities extracted from the profiles in the soft sediments are presented in Appendix A-2. A summary plot of interval shear wave velocities (Vs) versus depth is presented in Figure 7, showing a range of velocities in the sediments from 80 m/s in the very near surface, to greater than 300 m/s at depths of $60^{+}$ m. A high velocity surface crust (200 – 250 m/s) is present in the upper 5 - 8 m that is attributed to gravel road bed compaction (0 - 0.5 m) and freeze-thaw cycles over the past several thousand years (1 – 8 m). The data indicate there is an increasing trend in velocity as the profiles advance west (and downslope) towards the Ottawa River. Interpretation of these sections will be undertaken as future research, but velocities have been extracted from the profiles. The downhole Vs log, located on the east side of Breckenridge Creek, is plotted with the reflection data, and indicates a good agreement with the velocities of the eastern profile (Figure 7).

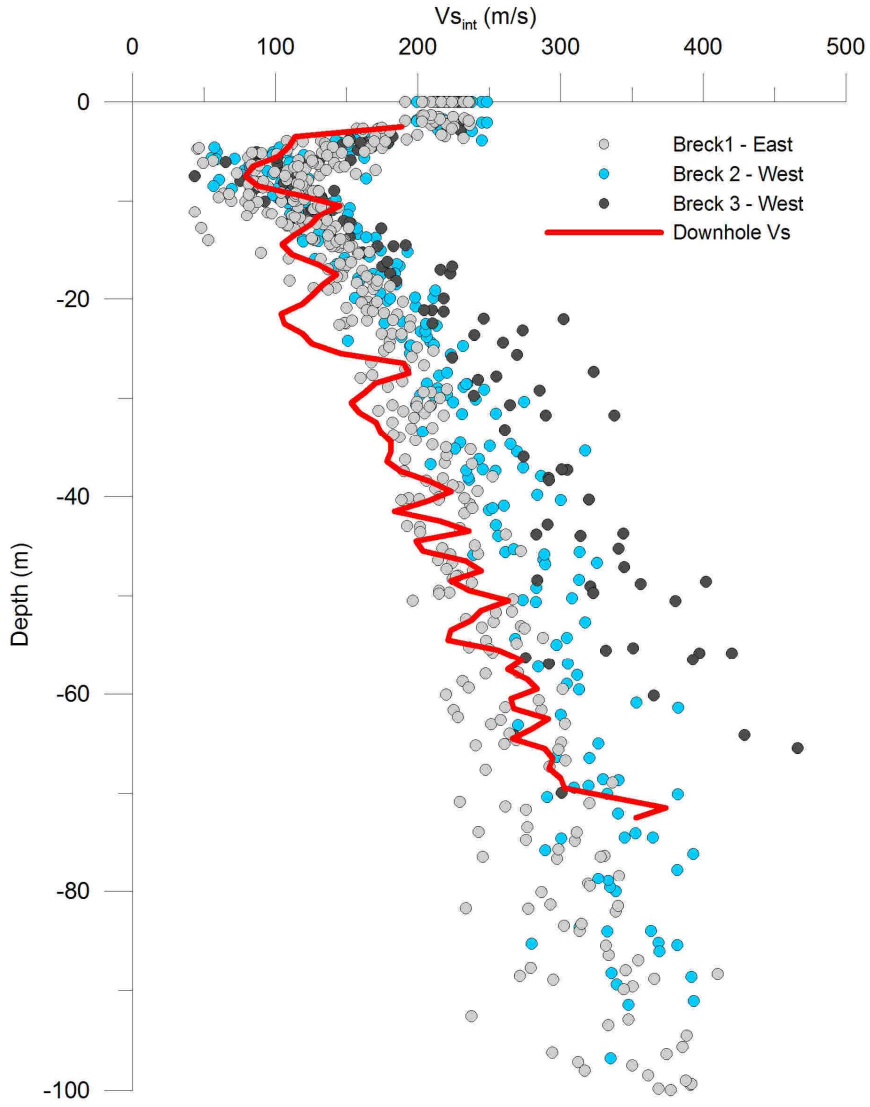


**Figure 7.** Shear wave interval velocity (Vs) of Champlain Sea sediments plotted against depth from the minivibe surveys. Downhole Vs (GSC-BRK-03), located on the east side of Breckenridge Creek, is plotted for comparison.

**Table 3.** Processing flow for seismic data.

| **Preliminary processing:** |
|---|
| Data conversion from SEG2 to processing software format |
| Prewhitening automatic gain control (AGC) to 1000 ms |
| Wavelet based deconvolution using the input sweep |
| Component separation |
| Geometry definition |
| Removal of noisy/dead traces |
| Common midpoint binning |
| |
| **S (H1-component) processing:** |
| Band pass filtering |
| Automatic Gain Control (AGC) scaling on an 800 ms window |
| Velocity analysis |
| Normal Moveout (NMO) correction |
| Common Midpoint (CMP) Stacking |

### 2.3 Borehole drilling and sampling

Based on the bedrock contour map (Figure 4), a drilling location was selected near the deepest part of the basin. Soil logs from the three Breckenridge boreholes are found in Appendix A-3, and basic borehole parameters are presented in Table 4.

**Table 4**. Basic borehole parameters. UTM zone 18. ID = Inner diameter.

| BH Name | Easting (m) | Northing (m) | Depth (m) | Borehole diameter (mm) | Casing Type, ID (mm) |
|---|---|---|---|---|---|
| BH-GSC-BRK-01 | 427 827 | 5 037 272 | 30.7 | 203 | PVC, 76.2 |
| BH-GSC-BRK-02 | 427 836 | 5 037 276 | 31.1 | 203 | Backfilled |
| BH-GSC-BRK-03 | 427 819 | 5 037 276 | 74.5 | 114 | PVC, 76.2 |

**Drilling and casing installation**

Borehole BH-GSC-BRK-01 was drilled to sample the silty clays of the upper 30 m, and to case a hole to allow for geophysical logging. The borehole was drilled on November 15 & 16, 2010 using a track mounted CME drill rig, advancing 115 mm (4.5") hollow stem augers (203 mm (8") outer diameter) (Figure 8a). An Osterberg hydraulic piston was used to recover 73 mm undisturbed samples using thin-walled (1.7 mm) Shelby tubes at approximately 4 m intervals (Figure 8b). To allow for geophysical logging, a 76.2 mm (3") diameter PVC pipe (in 305 cm (10') threaded sections) was cemented in place using Type 10 GU grout. The bottom of the PVC stem was capped and no screen was installed.

Borehole BH-GSC-BRK-02 was drilled to a depth of 31.1 m on March 25, 2011 using a track mounted CME drill rig, advancing 203 mm (8") hollow stem augers (254 mm (10") outer diameter). An Osterberg hydraulic

piston was used to recover 152 mm undisturbed samples using specially designed thin-walled (1.6 mm) Shelby tubes at approximately 3 m intervals. The borehole was backfilled with native sediments and not cased.

In 2014, borehole BH-GSC-BRK-03 was drilled and PVC-cased to investigate the nature of the glaciomarine sediments deeper in the bedrock basin, and for ground truthing of HVSR and seismic reflection data. This borehole was drilled to a depth of 75 m between March 10 and 19, 2014, using a track mounted CME drill rig, advancing 115 mm (4.5") (HQ) casing using mud rotary methods (Figure 8c). An Osterberg hydraulic piston was used to recover 76 mm undisturbed samples using thin-walled Shelby tubes at 3 m intervals to a depth of 63.90 m. Due to the increasing presence of sand at that depth, it was decided to stop sampling and flushing, and advance the drill rods slowly, carefully assessing for indications of artesian conditions which were known to exist in the region. As HVSR measurements at the site indicated the main resonator (bedrock or till) would be encountered at approx. 85 m, drilling was stopped at 75 m to avoid intersecting any coarse grained sediments under possible artesian pressures. To allow for geophysical logging, a 76.2 mm (3.0") diameter PVC pipe (in 305 cm (10') threaded sections) was cemented in place using Type 10 GU grout with 5% bentonite. To ensure the grout was evenly distributed, liquid grout was pumped inside the metal casing stem and the threaded PVC casing (with a bottom cap) was pushed into the grout to a depth of 74.5 m. The metal casing was then retracted, allowing the grout to flow into the borehole annulus. Over the first week, settlement of the grout occurred to a depth of approximately 24 m and the drillers returned to the site to top up the grout to ground surface. Basic borehole logs and sample intervals are presented in Appendix B-1 (Soil Log_GSC-BH-03.PDF).

**Sample preservation, transport and storage**

Shelby tube samplers were retrieved, cleaned, and tube ends waxed immediately on site to prevent moisture loss. GSC practices for waxing samples are based on ASTM standard D4220, and involve repetitive coating of tube ends in a mixture of beeswax and 25% petroleum jelly to decrease the brittleness of the wax once hardened. A total of twenty thin-walled Shelby tubes were recovered and sealed. Three glass sample jars were collected at depths where a Shelby tube failed to retrieve a full sample, but enough core was recovered for a grain size analysis. Samples were stored upright in insulated wooden boxes lined with foam (Figure 8d). Each evening, samples were transported back to GSC soil refrigerators, where they were stored upright in their transport boxes at 5°C until extruded in the lab.


**Figure 8.** (a) Drilling BH-GSC-BRK-01 (Nov 2010) using hollow stem augers and a track mounted rig. (b) hydraulic Osterberg piston sampler and thin walled Shelby sample tube. (c) Drilling BH-GSC-BRK-03 (2014) using a track mounted rig and mud rotary techniques. (d) Preserved sample tube ends coated in multiple layers of wax, stored upright for transport to GSC soil refrigerators.

## 2.4 Borehole geophysical logging

Downhole geophysical logs provide a means of identifying and characterizing lithological units based on variations in their chemical and physical properties. Geophysical logs also augment geological logging by providing information on changes in sedimentary properties that may not be visible in the core (e.g. subtle grain size changes, variation in pore water conductivity), and allow for the interpretation of measured geotechnical properties across soil intervals that were not sampled.

Downhole logging techniques included gamma methods (natural gamma and gamma-gamma density), induction methods (apparent conductivity and magnetic susceptibility), and downhole shear wave seismic methods. Table 5 describes the basic parameters of the downhole tools. A more detailed description of the tool theory can be found in Crow et al. (2015). The downhole geophysical log data from GSC-BH-BRK-03 are presented in Figure 9, and displayed alongside the lab-measured data in Appendix A-3 (GSC-BH-BRK-03.pdf).

**Downhole field procedures**

Geophysical logging was carried out on June 20$^{th}$, and July 3-4$^{th}$, 2014. Gamma and induction logs were acquired using a Mount Sopris logging system with a Matrix console and interchangeable downhole probes. A laptop computer recorded the data using Matrix Logger software. Prior to departure for the field, laboratory calibrations were performed with the gamma-gamma density tool using specially designed blocks of 1.28 and 2.60 g/cm$^3$ to provide low and high density calibration points. On-site calibrations were carried out with the conductivity and magnetic susceptibility tools prior to each run using known calibration points (for conductivity: low: 0 mS/m, high: 1690 mS/m; for magnetic susceptibility, low: 0 ppt, high: 300 ppt). All logs were corrected for sensor offsets and casing stick up, and recorded relative to ground surface.

The shear wave survey was carried out using a downhole 3-component (3-C) wall locking tool with 15 Hz omni-directional geophones, connected to a Geometrics Geode seismograph. The source consisted of a hammer striking an angled metal plate coupled with the ground, located 4 m from the borehole collar. The cable supporting the receiver array was lowered by hand to the bottom of the hole and pulled uphole at 0.50 metre spacings, where stationary measurements were made. The data were recorded on a laptop computer after reviewing each record on screen. Stacking of the signal was not deemed necessary as the signal-to-noise ratio was high and the reflections were very clear. Additional information on the systems, field procedures, and processing methods developed for downhole S-wave logging are described in detail in Hunter et al. (1998) and Hunter and Crow (2015).

**Downhole data processing**

Geophysical log data were imported into WellCAD software for processing and interpretation. As logs were recorded relative to ground surface, depth adjustments were not required during post processing. As a measure of quality control, upward and downward runs were overlaid to check for tool-induced temperature drift and to ensure repeatability.

To account for deviation from linearity in EM39 measurements as sediment bulk conductivity increases, a correction was applied to the conductivity log using the calibration curves presented in Geonics' EM39 operating manual (Geonics, 2006). A correction was also applied to the EM39S log based on the corrected EM39 log (pers. comm., D. McNeill, Geonics, 1984).

**Table 5.** Basic downhole geophysical log parameters.

| **Geophysical log** ***[Manufacturer]*** | **Logging unit** | **Radius of investigation** | **Logging speed** | **Logging interval** | **Practical interpretations** |
|---|---|---|---|---|---|
| **Apparent Conductivity (EM39)** *[Geonics/Mount Sopris]* | MilliSiemens/ metre (mS/m) | 0.3 m | 3 m/min | 0.02 m | Formation conductivity, (grain and/or pore water conductivity) |
| **Magnetic Susceptibility (EM39S)** *[Geonics/Mount Sopris]* | Parts per thousand SI (ppt SI) | 0.3 m | 3 m/min | 0.02 m | Magnetite (heavy mineral) concentration |
| ***Natural Gamma*** *[Mount Sopris]* | Counts per second (cps) | 0.3 m | 1 m/min | 0.01 m | Variation in grainsize and mineralogy |
| **Calibrated Gamma-gamma Density (Cs-137 source)** *[Mount Sopris]* | Counts per second (cps) calibrated to $g/cm^3$ | 0.15 – 0.25 m | 1 m/min | 0.02 m | Density of materials surrounding well |
| **Shear (S) Wave** *[Geostuff]* | Metres/second (m/s) | metres | Stationary readings | 0.5 m | Compaction, reflecting horizons |

The gamma-gamma density log in unconsolidated sediments is influenced by the presence of the PVC casing and grout surrounding the casing. To correct for this effect, log densities below 25 m were compared with calculated densities from the cores. Using a grain density of 2.80 $g/cm^3$ (based on the weight percent mineralogical analyses of the fine sediments), an average fluid density of 1.0 $g/cm^3$, and known porosities from the water content data, densities were calculated and compared to the gamma-gamma log data. The differences between these two density data sets ranged between 0.09 - 0.22 $g/cm^3$ (with an average of 0.16 $g/cm^3$) and were found to generally have a decreasing trend with depth. Therefore, a depth-based linear equation was developed for this site which corrected the gamma-gamma density log and compensated for the influence of the grout. After correction, good agreement was found between the two data sets, allowing for density measurements between sample intervals and below the last sampling depth at 63.4 m.

Unfiltered single fold S-wave travel times were picked using Interpex software at the onset of the shear wave arrival. A three point weighted-average filter was applied to the travel times, and interval velocities were computed using the difference in travel time (dT) between successive readings divided into the difference in

depths (dZ) between station depths. The distance between the source and the downhole tool was computed using the hypotenuse of the tool depth downhole and the source-borehole collar distance (4 m).

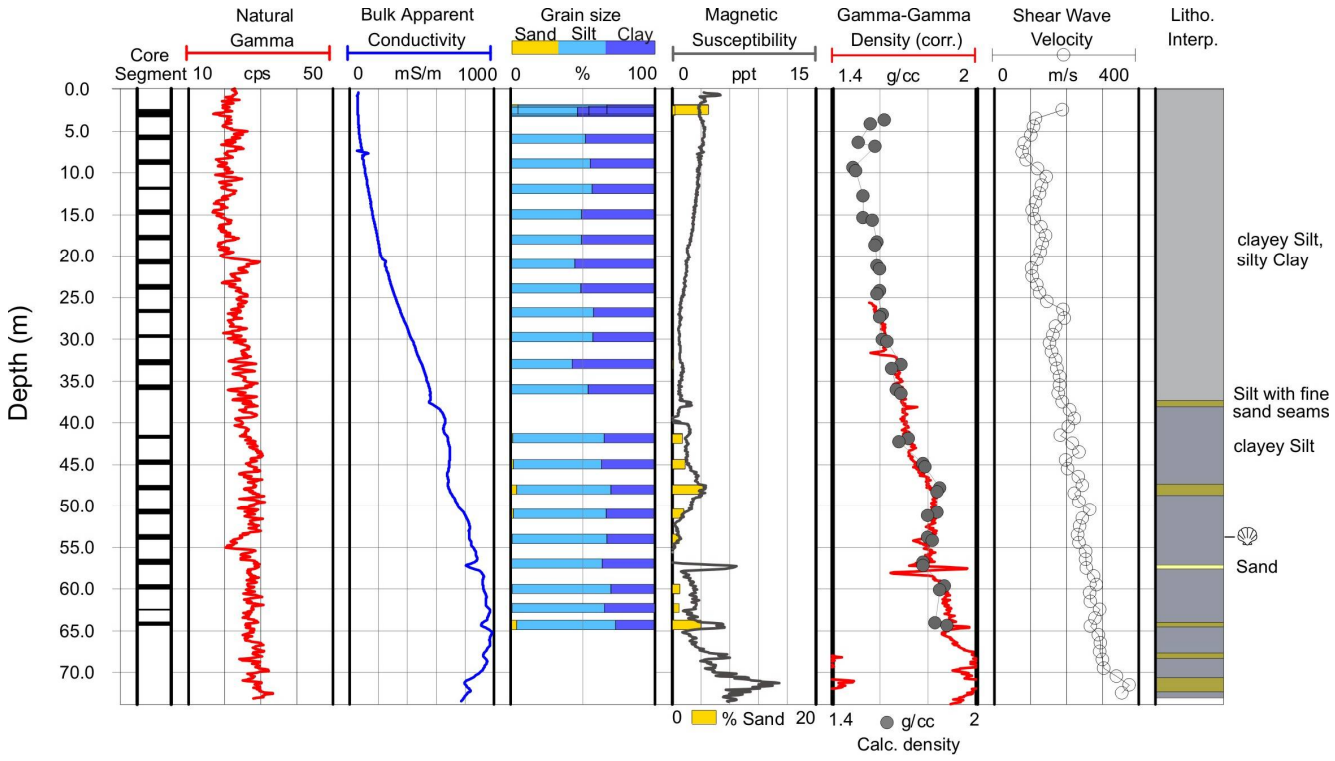


**Figure 9.** Borehole geophysical logs from GSC-BH-BRK-03. Calculated density derived from water content measurements from sediment samples. Lithological interpretation based on combined geophysical logs, core examination, and grain size analyses. The shell icon on the lithology column identifies the depth of a fragment found in core segment 19. Genus identification and age dating are discussed in Section 3.4.

## 2.5 Electrical resistivity profiling

A galvanic resistivity (GR) survey involves injection of current into the ground via contact with a pair of current electrodes. The potential distribution is then measured across many pairs of voltage electrodes and an electrical resistivity model is constructed that adequately honours the data (e.g. Loke et al. 2013). The measurements are moved along the survey line using electronic switching controlled by a resistivity meter.

Four profiles were collected in the Breckenridge Creek area between July 8 – 14th, 2014 (Figure 2, Table 6). Two of the profile alignments were chosen to cross borehole GSC-BH-BRK-03 so that downhole apparent conductivity values could be compared with the inverted resistivity (conductivity) values and extrapolated along the survey lines. On Lines 1, 2, and 4, the profiles were extended from the field over the eroded terrains which led down to Tributary A to investigate whether a significant variation in conductivity could be seen when approaching creek margins.

**Table 6**. Line locations for the four electrical resistivity profile lines collected near Breckenridge Creek.

| Line number | Start electrode UTM Zone 18 | | End electrode UTM Zone 18 | | Line length (m) |
|---|---|---|---|---|---|
| | Easting | Northing | Easting | Northing | |
| 1 | 427842 | 5037275 | 427625 | 5037372 | 475 |
| 2 | 427110 | 5036989 | 427454 | 5037034 | 355 |
| 3 | 427827 | 5037150 | 427791 | 5037815 | 655 |
| 4 | 427594 | 5037790 | 427824 | 5037770 | 235 |

**Data collection**

Data were collected using a 48-electrode resistivity meter (IRIS Syscal R1+ Switch) with 5 m electrode spacings and 0.3 m stainless steel electrodes (Figure 10 a, b). The 48-electrode measurement sequence consisted of 509 measurements collected at 0.5 Hz and stacked 3 times. Electrode geometry was in-line dipole-dipole with the following dipole lengths and depth spacings: $a$ = 5 m, $n$ = 1, 2, 3, 4, 5; $a$ = 15 m, $n$ = 5/3, 7/3, 3, 11/3, 13/3, 5; and $a$ = 25 m, $n$ = 16/5, 18/5, 4, 22/5, 24/5, 26/5. Larger dipoles and lower $n$-spacings often result in better signal strength than smaller dipoles at high $n$-spacing without significant loss of resolving capability in the inversion. While not optimized, the non-standard fractional $n$-spacings allow for more uniform depth coverage and overlapping potential dipoles, the latter of which has been shown to add information content to the inversion (Stummer et al., 2004). The geometry selected for these surveys was designed for a nominal maximum investigation depth of approximately 40 m.

Lines 1, 2, and 3 were "rolled" several times to extend the length of the line by moving the first 24 electrodes to the end of the line. Contact resistance checks on Lines 1, 3, and 4 were all under 3 kOhm. On Line 2, contact resistance checks on the first 14 electrodes exceeded 10 kOhm due to a resistive sandy cap in the near surface. One foot holes were dug for the electrodes (Figure 10 c, d) which were then salted, reducing the resistances to 2-5 kOhm, allowing the survey to proceed.

**Data processing**

Survey geometry was assigned to the acquired data, which involved translation to a prescribed coordinate system and assignment of topography. In the case of 2D GR data collected with a multicore cable, processing is done in terms of survey lines and distance along the cable (along the ground). For each line, GPS coordinates were acquired for at least the first and last electrodes and also any important positions along each line. The initial processing step involved thorough examination of the data along with field notes; obvious outliers and data associated with any non-contact electrodes were eliminated along with low-voltage data (<0.05 mV) and data with poor repeatability (<3%). Given the relatively high conductivities encountered in the survey, in combination with current and power limitations of the instrument, measured potential differences were typically below several mV with injected currents of several hundred mA.


**Figure 10**. Breckenridge Creek resistivity surveys. (a) The IRIS Syscal resistivity unit. (b) Survey along Line 3 on the edge of a field. (c) Electrode dug into the sandy soil along profile Line 2. (d) Line 2 is flanked on either side by prehistoric landslides, and terminates at the backscarp of a slide which occurred in 2008.

The GR potential data were then used for electrical resistivity imaging (ERI) of the subsurface via the iteratively re-weighted least squares inversion method of Loke et al. (2003). Data with greater than 10% misfit were re-weighted to reduce the effect of data that were inconsistent with the inversion. A large Ekblom perturbation of 0.1 was used to approximate a "soft" $L_1$ norm on the model that results in both smooth and

blocky features to some extent (Farquharson and Oldenburg, 1998). Given the diffusive nature of the target (salt concentration) a full $L_1$ norm on the model is not appropriate. Logarithmic transformations were used on both the data and the model, and no bounds were placed on the recovered model values. The model cell dimensions (horizontal and vertical) were set at one-half of the electrode spacing such that cell size should not significantly affect inversion results. The regularization parameter was cooled from 0.20–0.04 and convergence was defined as less than 7% change in the data misfit or a prediction error below 4% which is on par with the maximum acceptable repeatability of the GR data (experimental noise often exceeds observed repeatability). Model regularization was set to recover models with 2:1 horizontal-to-vertical smoothness and maximum resolvable depth was taken as the limit of 0.5% of the maximum resolution per area although this measure does not account for model non-uniqueness (Oldenborger and LeBlanc, 2015). Artefacts associated with surface topography and survey line curvature are evident in the ERI results.

Figure 11 presents the results of the inverted resistivity profiles. The approximate depth of investigation is shown on the sections with a black line. The trend seen in lines 1, 3, and 4 is in agreement with observations from the downhole conductivity log, where relatively low conductivities (high resistivities) in the near surface smoothly transition into higher conductivities (low resistivities) at depth where pore waters gradually become more conductive. Line 2, collected along a path flanked on either side by prehistoric landslides and terminating at the backscarp of the 2008 landslide (Figure 10d), indicates resistivities are more elevated deeper in the profile than is seen in the other lines.

In comparing the apparent conductivity log from BH-GSC-BRK-03 to the ERI conductivity model where it passes the borehole, the log is typically greater than the ERI conductivity by a factor of 2. This discrepancy may be due to macro-anisotropy (layering) or EM39 calibration. EM39 provides a measure of horizontal conductivity, whereas ERI provides a measure of the geometric mean. As such, the observed conductivities suggest a vertical:horizontal resistivity ratio of 4:1 if all of the discrepancy is attributed to anisotropy. The cause of this discrepancy between the two techniques is a topic of future research within the Champlain Sea sediments in the region.

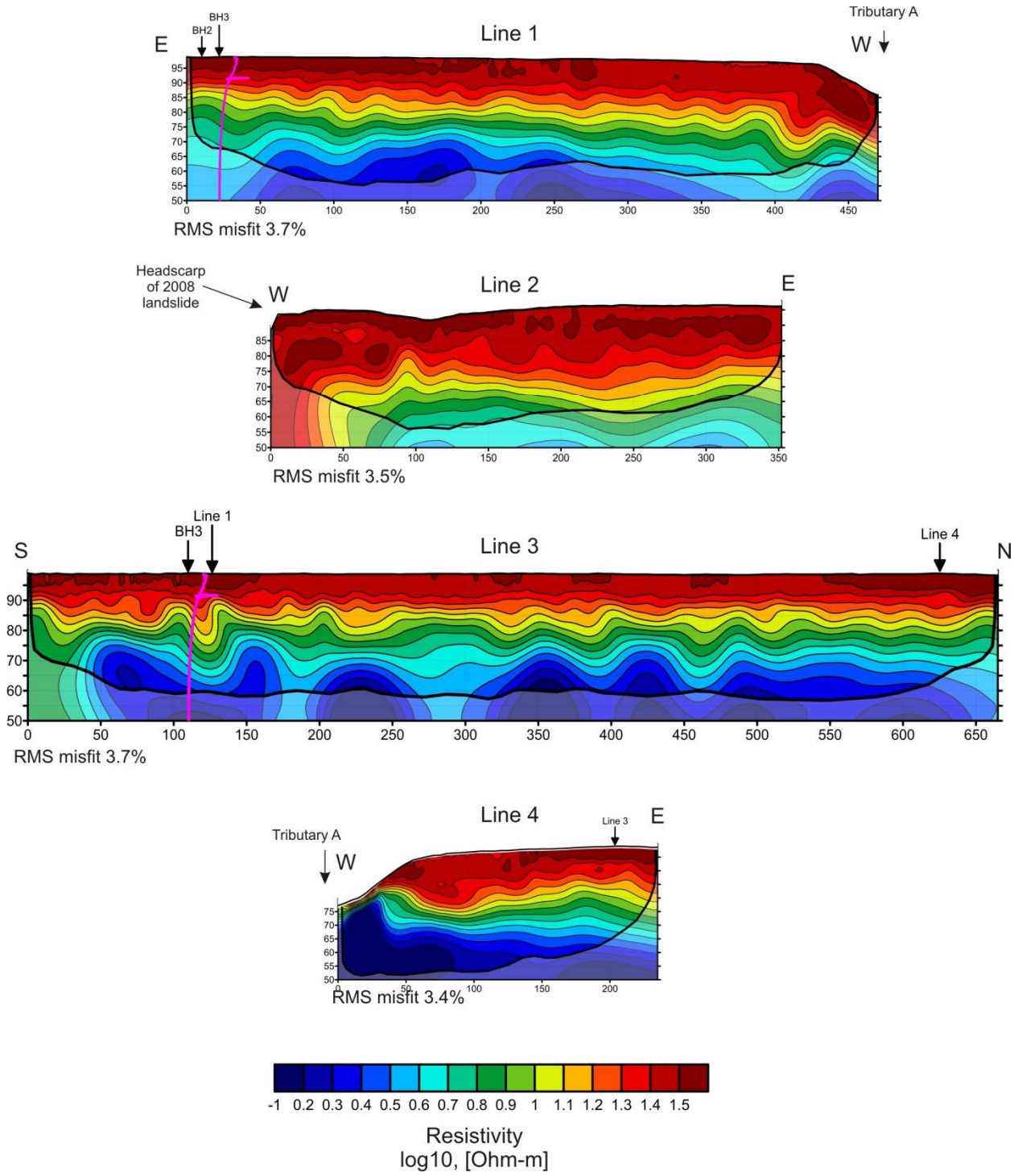


**Figure 11**. Inverted electrical resistivity profiles collected in the Breckenridge Creek study area. The black line indicates the approximate depth of investigation. Lines 1 and 3 show the position of borehole GSC-BH-BRK-03 along the profile.

## 3.0 Laboratory testing of samples from BH-GSC-BRK-03

Laboratory analyses on cores recovered from BH-GSC-BRK-03 were conducted by the Geological Survey of Canada in Ottawa, with the exception of the isotopic analyses that were carried out by the University of Waterloo. Core descriptions, grain size analyses, moisture content, Atterberg limits, pore water exaction, and mineralogy studies were all performed by the GSC's Mineralogy and Physical Properties (MPP) Laboratories. Chemical analyses of pore water analytes were completed by the Inorganic Geochemistry Research Laboratories – Environment (IGRL-E). This section provides a description of the lab techniques, with results presented in Tables B-1 and B-2 found in Appendix B. Results are also presented alongside the geophysical logs in Appendix A-3 (GSC-BH-BRK-03.pdf).

Preserved samples from BH-GSC-BRK-01 and -02 were distributed to Laval, Carleton, and Waterloo universities as part of a larger collaborative study investigating Champlain Sea sediment behaviour at four sites in the Ottawa and St Lawrence river valleys (Crow et al., 2013). Lab work consisted of basic geotechnical characterization (Atterberg limits, sensitivity from fall cone testing, grain size analyses (using hydrometer for silt-clay sized particles), oedometer testing, and analyses of mechanical behaviour under static and cyclic loading using direct simple shear and cyclic triaxial testing, respectively. Results of these geotechnical tests at the Breckenridge site can be found in a Master's thesis completed by Duguay-Blanchette (2016).

### 3.1 Physical properties

#### 3.1.1 Core extrusion, description, and subsampling

Physical property measurements were conducted immediately upon extrusion from the core tubes in April 2014. Using a hydraulic piston designed for extraction, the core sediment was carefully extruded into clean sample trays lined with clear plastic wrap. Cores were immediately measured and photographed (Appendix B-1). The upper end of the tube often contained a few centimetres of remoulded material which entered the tube during the sampling process; this material was removed prior to photography. Cores numbers, depths (top, bottom), and other basic information are presented in Table 7.

Cores were geologically logged, noting the Munsell soil colour in natural light conditions. A description of soil stiffness, moisture, texture, and presence of hydrotroilite (a black, amorphous ferrous sulphide, e.g. www.mindat.org) and sand seams were noted. Core segments were then sub-sampled for various tests including grain size (2 per core segment), moisture content (2 per core segment), fall cone (1 per core segment), Atterberg limits (1 per core segment), and pore water extraction (1 per core segment). A 10 cm sample from each core segment was retained for future re-testing.

The samples were remarkably consistent in colour, varying subtly from the top to the bottom of the borehole. Samples appeared homogenous in texture without visible red-grey banding as has been reported by Percival et al. (2001). Some very faint grey banding was only noted in core segment 14. Black hydrotroilite bands (1 – 2 cm) were first observed in core segment 7. These bands, and dark hydrotroilite flecks, persisted in the cores to segment 22, but were not observed in the final core segment 23. Fine sand lenses were first identified in segment 17, and were also present in segments 21 and 23. Tiny white remnants of *Portlandia arctica* shells were noted in segments 15, 19 and 20.

In addition to the above mentioned tests, two small samples of sand from segments 21 and 23 were extracted for X-ray powder diffraction (XRD) analysis to identify their mineralogy. Verification of certain trace minerals was made using the scanning electron microscope (SEM) on grain mounts. Three samples of silt from core segments 5, 13, and 22 were also selected for XRD analyses to investigate mineralogy and potential variation with depth.

**Table 7.** Core segment numbers, depth intervals, and basic colour descriptions of sediments.

| Core Segment | Depth Interval (m) | (m) | Container Type | Munsell Colour | Munsell Description |
|---|---|---|---|---|---|
| 1 | 2.40 | 2.50 | Glass jar | - | - |
| 2 | 2.50 | 2.60 | Glass jar | - | - |
| 3 | 2.60 | 3.24 | Shelby tube | 5Y 5/1 | Grey |
| 4 | 5.40 | 5.96 | Shelby tube | Gley 1, 4/1 10Y | Dark Greenish Grey |
| 5 | 8.40 | 8.92 | Shelby tube | Gley 1, 4/1 10Y | Dark Greenish Grey |
| 6 | 11.70 | 11.94 | Shelby tube | Gley 1, 5/1 10Y | Greenish Grey |
| 7 | 14.40 | 14.95 | Shelby tube | Gley 1, 4/1 10Y | Dark Greenish Grey |
| 8 | 17.40 | 18.00 | Shelby tube | Gley 1, 4/1 10Y | Dark Greenish Grey |
| 9 | 20.40 | 20.94 | Shelby tube | Gley 1, 4/1 10Y | Dark Greenish Grey |
| 10 | 23.40 | 23.96 | Shelby tube | 5Y 4/1 | Dark Grey |
| 11 | 26.40 | 26.78 | Shelby tube | Gley 1, 4/1 10Y | Dark Greenish Grey |
| 12 | 29.40 | 29.74 | Shelby tube | Gley 1, 4/1 10Y | Dark Greenish Grey |
| 13 | 32.40 | 33.01 | Shelby tube | 5Y 4/1 | Dark Grey |
| 14 | 35.40 | 36.02 | Shelby tube | 5Y 4/1 | Dark Grey |
| 15 | 41.40 | 41.85 | Shelby tube | Gley 1, 4/1 5GY | Dark Greenish Grey |
| 16 | 44.40 | 44.96 | Shelby tube | Gley 1, 4/1 10Y | Dark Greenish Grey |
| 17 | 47.40 | 48.00 | Shelby tube | Gley 1, 4/N | Dark Grey |
| 18 | 50.40 | 50.97 | Shelby tube | Gley 1, 4/N | Dark Grey |
| 19 | 53.40 | 53.98 | Shelby tube | Gley 1, 4/N 10Y | Dark Grey |
| 20 | 56.40 | 57.01 | Shelby tube | Gley 1, 4/1 10Y | Dark Greenish Grey |
| 21 | 59.40 | 59.99 | Shelby tube | Gley 1, 4/1 10Y | Dark Greenish Grey |
| 22 | 62.40 | 62.45 | Glass jar | - | - |
| 23 | 63.90 | 64.33 | Shelby tube | Gley 1, 4/1 10Y | Dark Greenish Grey |

### 3.1.2 Water content

Gravimetric water (or moisture) content tests were conducted within minutes of core extrusion from the Shelby tubes. A 2-cm piece of undisturbed sediment was selected from near the top and bottom of each sample tube, weighed, and oven dried for >24 hours at 105°C, following the standard established by the Standards Council of Canada CAN/BNQ 2501-170/2014. Water contents ranged between 40% and 99%.

Using standard soil mechanics relationships (e.g. Budhu, 2007), an assumed saturation (S) of 100%, and specific gravity ($G_s$) of 2.65, void ratio (e) and porosity (%) were then calculated using the measured water content of each sample. Porosities range between 0.73 (at 8.5 m) and 0.51 (at 64.3 m).

### 3.1.3 Grain size

To obtain a complete grain size distribution of the samples, two instruments were used. The classes of sizes greater than 63 □m were determined using wet sieving (to obtain the >45□□m to <2 mm size fraction) followed by dynamic digital image processing using a CAMSIZER Particle Size Analysis System. The classes of sizes smaller than 63□□m were determined using a Lecotrac LT-100 Particle Size Analyser.

### 3.1.4 Fall cone penetrometer measurements

The fall cone apparatus (see Hansbo, 1957), gives relatively precise information on the consistency of clays in intact and remoulded states. For these tests, a Roctest penetrometer was used, with a series of standard metal cones (10 g and 60 g (with 60° tip angle) and 100 g and 400 g (with 30° tip angle)). The chosen cone was suspended with its tip just touching the surface of a leveled intact clay/silt sample. When the cone was released, the penetration depth of the cone into the sample was measured and compared against a standard look-up table of shear strengths (in metric tonne/$m^2$). This test was repeated until the penetration of three consecutive tests were within ±0.5 mm, to ensure repeatability and uniformity of the sample. The sample was then remoulded using a clean metal spatula, and once a uniform consistency was reached, the sample was returned to a small porcelain dish, leveled, and the cone dropped into the sample once again. The tests were again performed three times to ensure repeatability, and the average penetration depth was used to look up the shear strength of the remoulded sample. Undisturbed shear strengths ranged between 20 – 126 kPa; remoulded shear strengths range between 0.5 - 26 kPa.

The ratio of the undisturbed ($C_U$) to remoulded ($C_R$) shear strengths is defined as the soil's geotechnical sensitivity ($S_T$), and ranged from 5 – 42. Numerous sensitivity scales exist (see L'Heureux et al. 2014); the Canadian Foundation Engineering Manual (2006) provides ranges of low (0-10), medium (10-40) and high sensitivity (40-100). By this scale, the sediments at the site are within the ranges of high and medium in the near surface (core segments 5 – 8), to medium to low (core segments 9 – 23). Segments 3-4 in the surface crust (<6 m depth) are of low to medium-low sensitivity.

### 3.1.5 Atterberg limits

The Atterberg limits are boundary measurements of a fine-grained sediment's water content in four different states: solid, semi-solid, plastic, and liquid. In each state, the consistency and engineering properties of the soil are different. Water contents at liquid and plastic limits are of particular interest for geotechnical investigations of clayey-silts, and their determinations are described below.

**Liquid limit (LL)**

The liquid limit (LL) is defined as the boundary between liquid and plastic states of a fine grained soil. Although the percussion method (as proposed by Casagrande, 1932) has been used extensively in the past for LL measurements, it is now recommended to use the fall cone method as the technique is proving generally more repeatable (Garneau and LeBihan, 1977; Wasti, 1987). The liquid limit, as measured by the fall cone, is defined as the gravimetric water content of the remolded clay that gives a 10 mm penetration of the standard 60

g, 60° cone. The techniques followed for this test are those established by the Standards Council of Canada CAN/BNQ 2501-092/2014. Liquid limits in the Breckenridge borehole ranged from 51 – 79.

**Plastic limit (PL)**

The plastic limit (PL) is defined as the boundary between plastic and brittle states of a fine-grained soil. The PL is determined by rolling out a thread of soil on a flat, non-porous surface, as described in ASTM Standard D 4318. The PL is said to be reached when soil rolled into threads of 3 mm begin to crumble when rolled under the palm of the hand. Gravimetric water content at this state is then determined, following the procedures described above in 3.1.2. Plastic limits ranged from 22 – 32.

**Plasticity index (PI)**

The plasticity index (PI=LL-PL) is a measure of a sediment plasticity, and typically increases with increasing content of clay-sized grains. PI ranged in the cores from 26 – 49.

**Liquidity index (LI)**

The liquidity index (LI=(W-PL)/(LL-PL)) scales sediment water content relative to plasticity, so that LI will be zero at the PL, and 1.0 at the LL. Many practitioners agree that retrogressive landslides will occur when remoulded shear strength <1 kPa and liquidity index >1.2 (e.g., Tavenas et al., 1983), and that these conditions are a better indicator of retrogression than sensitivity ($S_T$). These conditions are satisfied in core segments 5 and 6, with LI also above 1.2 in segment 7 (Cr=1.27 kPa) and Cr below 1.0 in segment 8 (LI=1.11). These results are in agreement with the presence of retrogressive landslides in the Breckenridge Creek study area.

## 3.2 Pore water analyses

Pore water chemistry can have a significant influence on the geotechnical properties of Champlain Sea sediments (e.g. Torrance, 1983). It also can provide valuable insight into the geochemical conditions present during sediment deposition, source water at the time of deposition, as well as physical and chemical processes influencing the development of the Champlain Sea.

### 3.2.1 Pore water extractions

Pore water was extracted from the samples in April 2014 by centrifuge using the innermost undisturbed portion of the core sections. Approximately 75 g of sediment were loaded into each 50-mL centrifuge tube. Samples were centrifuged at 13 000 rpm for 30 minutes at 5°C with 8 samples per run. A Heraeus™ Biofuge™ Stratos™ standard model centrifuge was used with a compatible Heraeus™ 8 x 50 mL fixed-angle rotor. After centrifuging, the supernatant was drawn off with an electronic pipette and placed into 4- or 8-mL high-density polyethylene (HDPE) vials, sometimes requiring more than one vial per sample. Samples 3 and 4 yielded 9-11 mL of pore water for each centrifuge tube. Samples 5 to 12 had pore water yields of 5-6 mL. The lowermost samples, 13-21 and 23, yielded 3-4 mL of pore water. The supernatant was clear from all pore water depth intervals and was devoid of suspended particulate; it did not require filtration or acidification for subsequent analyses (Figure 12). One distilled de-ionized water sample was also processed as a blank at the end of each centrifuge run.

Pore water was extracted again in 2016 from remaining segments of untested, refrigerated core that had been preserved in layers of plastic wrap and sealed plastic bags. Pore water was centrifuged and handled using the same procedures as noted above, although the sample depth intervals differed slightly from the 2014

extractions. Duplicate extractions were performed on samples 3, 13 and 17 using vertical slices along the same depth interval to provide replicate samples for quality control.

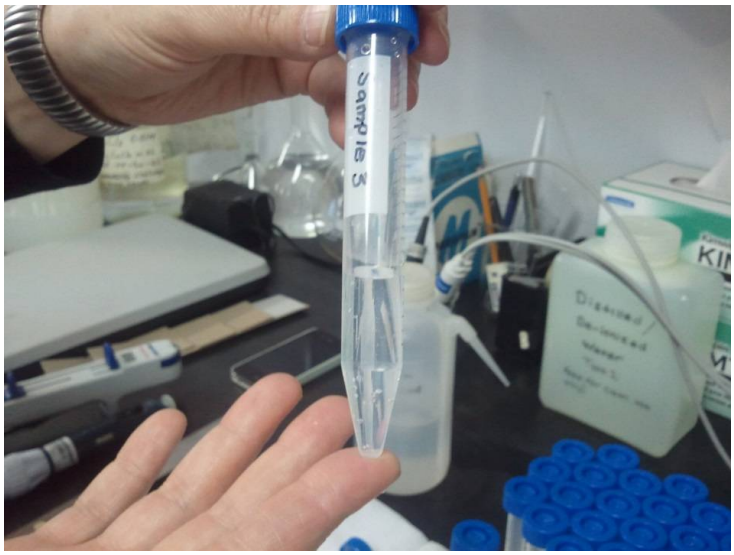


**Figure 12**. Clear supernatant extracted from core segment 3 (2.75-2.90 m depth) in 2014.

### 3.2.2 Geochemistry of pore water (Inorganic Geochemistry Research Laboratories, GSC)

Pore water samples from the 2014 centrifuging were used for the inorganic analyses. The fluids were unacidified, unfiltered, and kept refrigerated at 5°C in 4-mL HDPE bottles immediately after centrifuging and before analysis of total sodium (Na), chlorine (Cl), and bromine (Br), which are almost completely in the ionic species $Na^+$, $Cl^-$, and $Br^-$ in aqueous samples. Dilution factors of 1 to 50 were required as a function of concentration, which increased with depth down the core. Elemental analysis was done by a Spectro Arcos™ end-on plasma (EOP; or axial) inductively coupled plasma optical emission spectrometer (ICP-OES) using a 1% $CsNO_3$ buffer (1:5 ratio) as a matrix modifier with a Burgener Teflon™ Mira Mist Nebulizer (uptake rate of 1 mL/min) and a cyclonic spray chamber. The argon flow rates were: coolant 14.5 L/min; auxiliary 0.9 L/min; and nebulizer 0.8 L/min. The RF power was 1500 watts. Inter-element correction factors were applied as required to correct for spectral interferences. Detection limits were dependent on dilution factors (Table 8). Random samples were chosen as repeats. Control blanks were analyzed regularly as were certified standard solutions (ONTARIO-99, SLRS-5). Figure 13 presents plots of pore water measurements of specific conductance (at 25°C), Na, Cl, and Br concentrations as a function of depth. The maximum concentrations measured in core segment 23 from a depth of 64.1 m are approximately 60–70% of current sea water composition with a salinity of approximately 22.1. The downhole borehole conductivity log (discussed in section 2.4) indicates that pore water from core segment 23 (at 64.1 m depth) nearly coincides with the depth of maximum conductivity reached in the borehole at 65.2 m. The conductivity generally decreases (with minor fluctuations) to the base of the log at 73.5 m (see Figure 9 and GSC-BH-BRK-03.pdf in Appendix A-3).

**Table 8.** Dilution factors and detection limits of Na, Cl, and Br analysis in pore water from ICP-OES analyses.

| | Dilution factor | Na (ppm) | Cl (ppm) | Br (ppm) |
|---|---|---|---|---|
| **Detection limits** | 1 | 0.05 | 0.1 | 0.05 |
| | 2 | 0.1 | 0.2 | 0.1 |
| | 10 | 0.5 | 1 | 0.5 |
| | 50 | 3 | 5 | 3 |

### 3.2.3 Pore water conductivity

For the pore waters extracted in 2014, conductivity was measured on two different occasions. The first time, measurements were made immediately after pore water extraction using a Fisher Scientific™ Accumet™ AR50 conductivity meter with an Accumet™ epoxy four-cell probe (cell constant, K = 1.0 $cm^{-1}$; for a conductivity range of 10.0 - 2000 µS/cm) for the shallow-depth samples (core segments 3-6). Remaining core segments were analyzed similarly using a probe with a cell constant of K = 10.0 $cm^{-1}$ (for a conductivity range of 1.0 - 200 mS/cm). Calibrations were done with a single point standard (99.4 µS/cm, 1.413 mS/cm, and 9.991 mS/cm). Core segments with higher conductivity (segments 13-21 and 23) were diluted 5-fold with distilled de-ionized water. All measurements were made after samples, blanks, and standards reached room temperature. Pore water conductivity was measured by immersing the cell in the sample and allowing the reading to stabilize before recording the result. To avoid cross-contamination, the cell was rinsed with distilled, de-ionized water (first analysis) in between samples, shaking the remaining droplet out and wiping with a clean KimWipe™ before proceeding to the next sample. Measurements were auto-corrected to 25°C and are therefore reported as specific conductance at 25°C. Calibration standards were measured every 2-4 samples.

Sample dilution for conductivity measurements is invalid because conductance is not directly proportional to ionic concentrations (Miller et al., 1988). With decreasing concentration, each ion contributes proportionally more to the conductance of the aqueous solution and will result in an artificially elevated specific conductance when measured and multiplied by the dilution factor. For this reason, undiluted pore waters, which had remained in cold storage in the interim, were re-analyzed two years later to compare diluted and undiluted samples, using similar conductivity measurement protocols (probe with K = 1.0 $cm^{-1}$). For the second analysis (2016), calibration was performed on a single point standard, namely, the Fisher Scientific™ traceable conductivity standard certified reference material with a conductivity value of 10 000 µS/cm. A set of Oakton™ conductivity standards (1413 µS/cm, 2760 µS/cm, and 12.88 mS/cm) was also analyzed, along with blanks and certified reference water. A standard solution was re-analyzed after every 10 samples and at the beginning and end of each run. Repeat analyses were also done at a rate of 1 random repeat for every 10 samples. Blanks and a certified standard solution (ION-96.3) were analyzed on a regular basis. Between samples, the cell was rinsed with reverse osmosis de-ionized water, shaken and wiped with a clean KimWipe™ before proceeding to the next sample.

The second analysis of conductivity in undiluted pore water samples generally yielded lower values than in diluted samples as anticipated. However, the downhole trend showed discrete deviations from the original measurements (Figure 13a), which warranted reconsideration of the conductivity measurements. To assess the two sets of measurements, pore water conductivity was estimated from chlorine concentrations using the approach suggested by Lewis and Perkin (1981). The relationships between chlorinity and salinity [2], and between salinity and $R_{15}$ [3]

$$S\ (‰) = 1.80655\ Cl\ (‰) \qquad [2]$$

$$S\ (‰) = -0.08996 + 28.29729\ R_{15} + 12.80832\ R_{15}^2 - 10.67869\ R_{15}^3 + 5.98624\ R_{15}^4 - 1.32311\ R_{15}^5 \qquad [3]$$

were used to estimate $R_{15}$, which is the ratio of sample conductivity over Copenhagen standard seawater at a temperature of 15°C (Lewis, 1980). This value was then multiplied by the conductivity of Copenhagen standard seawater at a temperature of 25°C (53 050 µS/cm; Janz and Singer, 1975) to obtain the calculated specific conductance at 25°C for pore waters, assuming the ionic composition of seawater. The measured specific conductance is plotted as a function of the calculated value in Figure 14.

As noted previously, results from the diluted first analysis (core segments 13 to 21 and 23) plot higher than those from the undiluted second analysis (Figure 14). The results of the undiluted second analysis are generally closer to the specific conductances calculated from chlorinity (Figure 14). This result is consistent with the effect of dilution resulting in slightly elevated specific conductance in the first analysis. Direct measurements of pore water specific conductance also plot above the calculated values for less saline pore waters (samples 3-12). This difference likely occurs because the ionic composition for less saline water differs from that of seawater with a greater proportion of ions, such as $Ca^{2+}$, introduced from mixing with terrestrial sources of water or from cation exchange within clays (e.g. Martel et al., 1978). Therefore, the assumption of constant ionic composition of seawater doesn't hold for less saline waters and cannot be used to calculate specific conductance (e.g. Millero, 2013).

The deviations in specific conductance with depth re-analyzed from core segments 17 and 23 may be artefacts of pore water sample preservation over the two-year interval between analyses because the excursions do not manifest in other ions (Figure 13 b-d) and the measured values are well below the calculated specific conductance (Figure 14). The lower conductivity measured in samples # 17 and 23 in the second analysis in 2016 may have resulted from sorption of ions to the container walls during extended storage. Consequently, errors may exceed measurement uncertainties and neither the analyses done in 2014 nor in 2016 are entirely reliable due to the dilutions of samples 13-21 and 23 in the first analysis and the possibility of pore water sample preservation artefacts prior to the second analysis. To address these uncertainties, additional pore water was extracted from the remaining preserved core in 2016 and conductivity was re-measured.

The specific conductance of pore waters extracted in 2016 was measured similarly to the first two analyses. For the shallow cores segments (# 3-4), a glass probe was used (K = 1.0 $cm^{-1}$; for a conductivity range of 10.0 - 2000 µS/cm). Deeper core segments were analyzed with an epoxy probe (with K = 10.0 $cm^{-1}$; for a conductivity range of 1.0 - 200 mS/cm). Calibrations were done with a single point standard (10.0 mS/cm for cores 3-5 and 7-11, and 100.0 mS/cm for cores 12-21 and 23). Additional standards (0.100 mS/cm, 1.413 mS/cm and CRM ION-96.3 (0.860 mS/cm)) were used as supplementary quality control checks. Results from the 2016 extractions are plotted in Figure 15 along with both the 2014 and 2016 analyses of pore waters originally extracted in 2014.

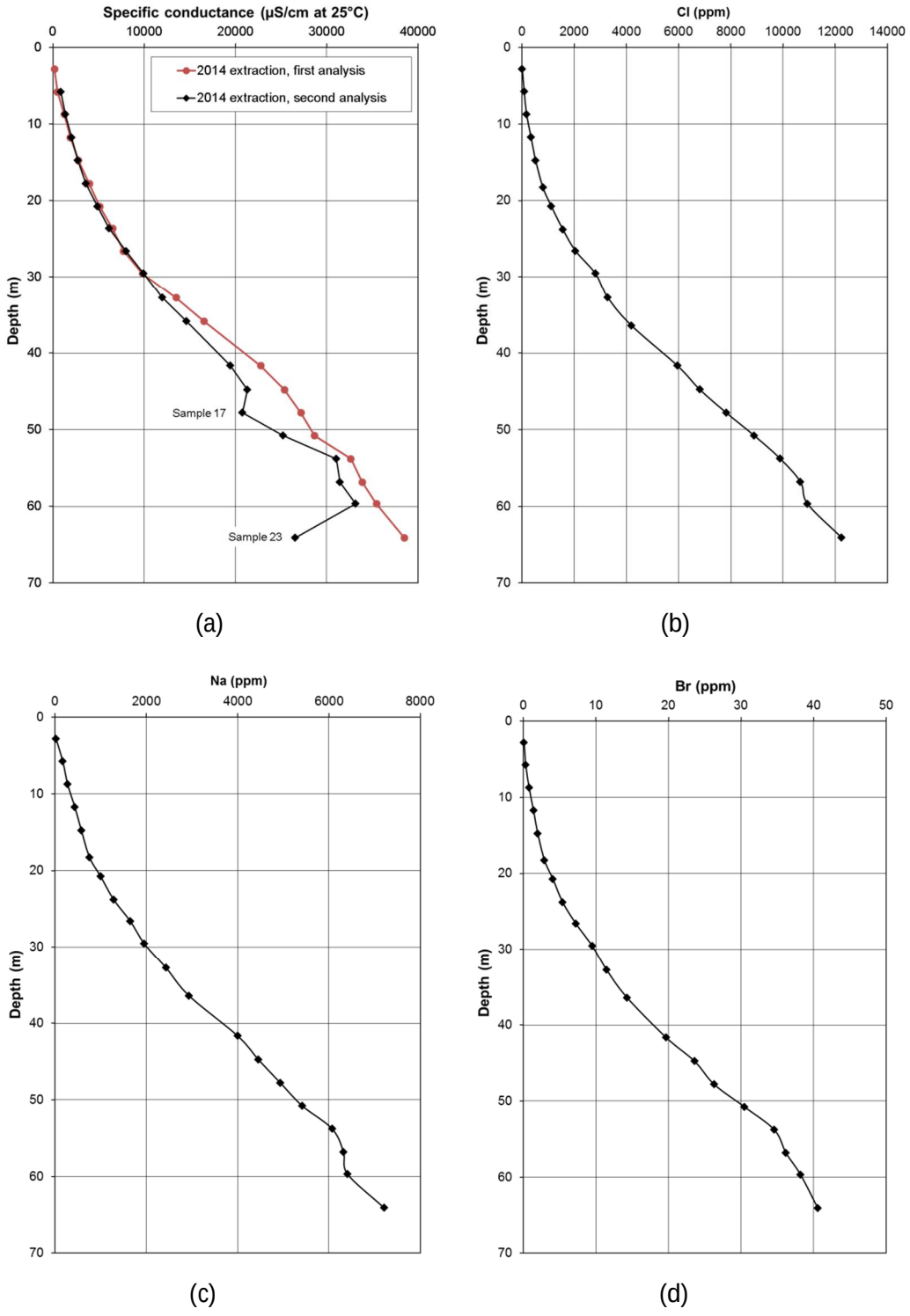


**Figure 13**. (a) Pore water specific conductance at 25°C (two analyses), (b) chlorine (Cl) concentration, (c) sodium (Na) concentration, and (d) bromine (Br) concentration as a function of depth.

The measured results are higher for the pore waters extracted in 2016 at low conductivities. Since lower conductivity pore waters are susceptible to storage artefacts as well (e.g. Torrance, 1976), results from the first analysis in 2014 are considered the most accurate because they were undiluted and had the shortest storage time.

At higher conductivities, the 2016 extraction results are lower than the results of the diluted samples from the 2014 extraction, as expected, but both sets of results follow a similar trend with depth. Results of the second analysis of the 2014 extractions are similar to the 2016 extractions at high conductivities except for core segments 17, 18 and 21. These findings give additional credence to the possibility of preservation artefacts for these samples (2014 extraction, second analysis). Furthermore, these results produce a depth profile similar in shape to those for Cl, Na, and Br (Figure 13 b, c, d). Therefore, the 2016 extraction results seem most appropriate at higher conductivity and are considered the most accurate. Figure 16 shows the optimal specific conductance results from these amalgamated analytical results – 2014 analysis on pore water extracted in 2014 for low-conductivity samples (<30 m depth) and 2016 analysis on pore water extracted in 2016 for high-conductivity samples (>30 m depth; Table B-2).

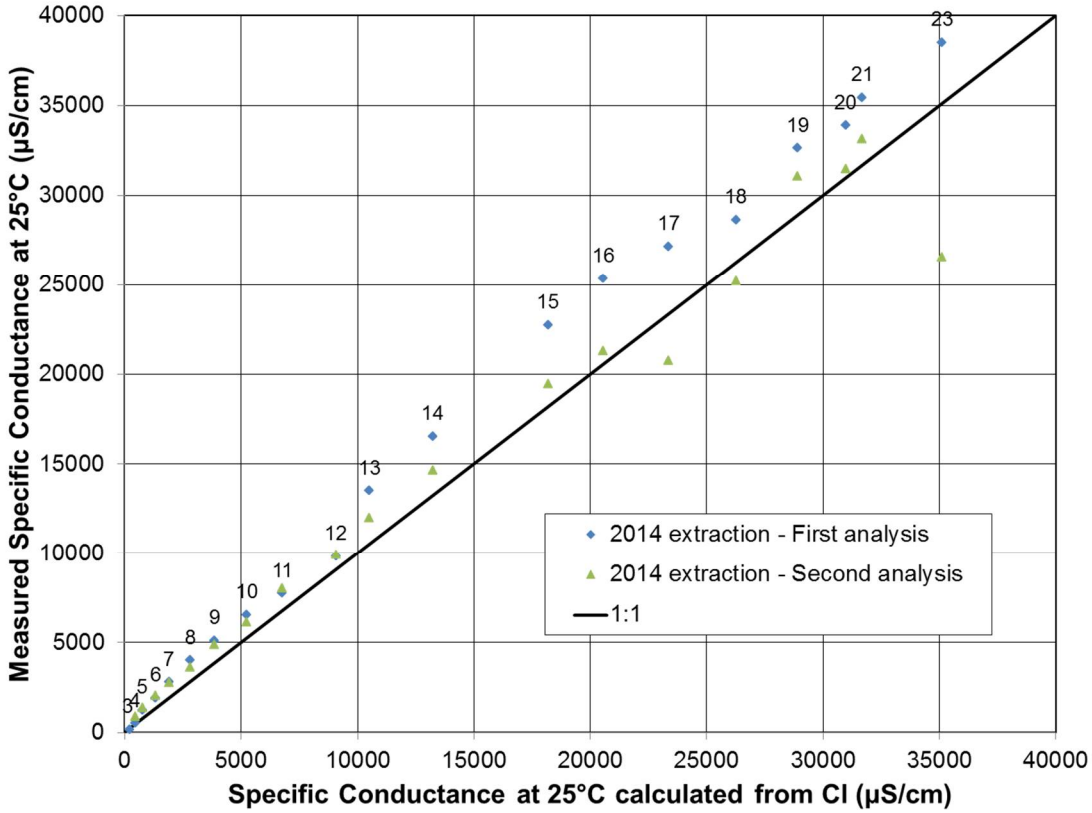


**Figure 14**. Comparison of two measurements of specific conductance versus specific conductance calculated using Cl results, assuming seawater composition. Labels indicate the core segment number.

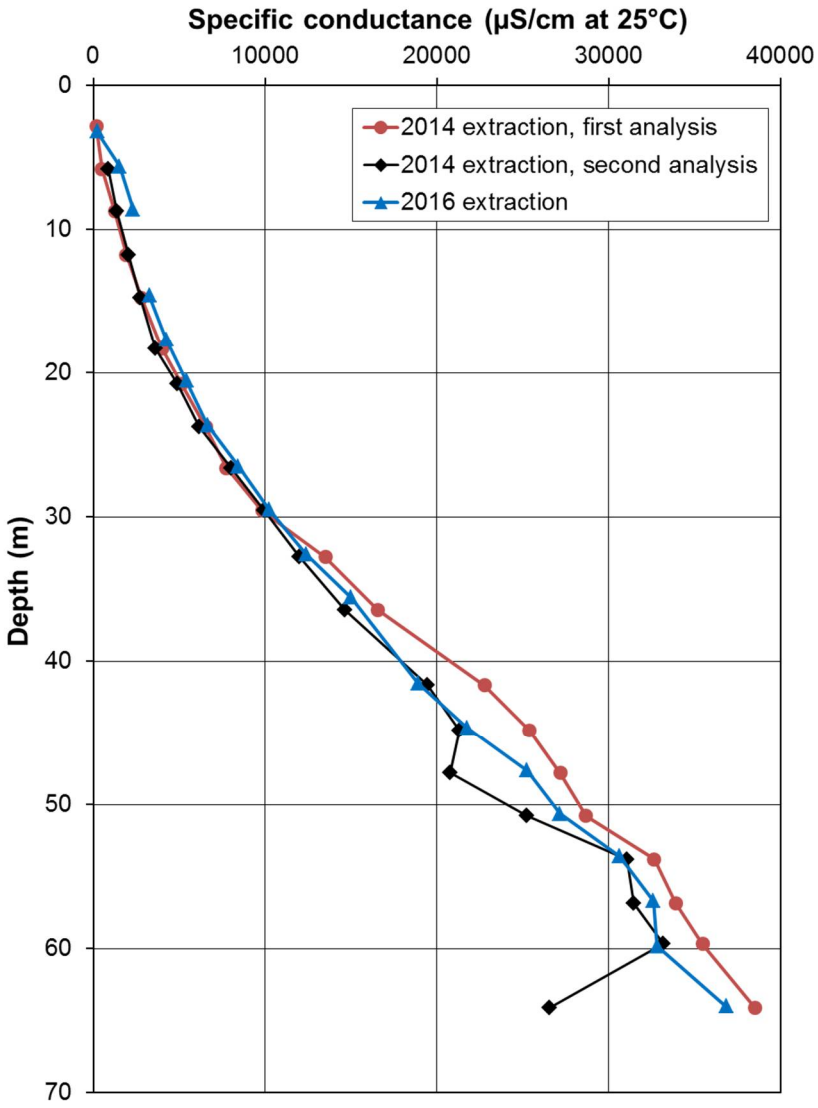


**Figure 15.** Pore water specific conductance at 25°C for 2014 and 2016 pore water extractions.

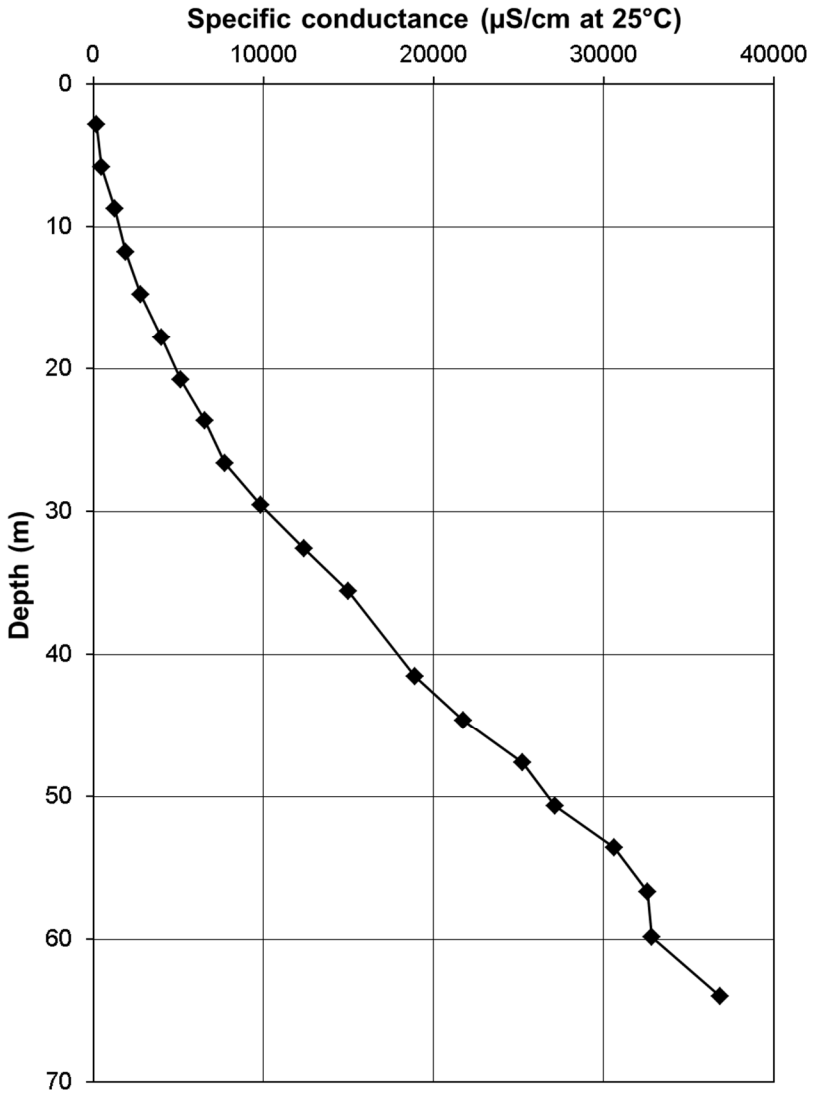


**Figure 16.** Composite pore water specific conductance at 25°C; 2014 analysis on pore water extracted in 2014 for low-conductivity samples (<30 m depth) and 2016 analysis on pore water extracted in 2016 for high-conductivity samples (>30 m depth; shown in Table B-2)

### 3.2.4 Isotopic analyses – direct analysis (Environmental Isotope Laboratory (EIL), University of Waterloo)

The ratios of the stable isotopes of hydrogen ($^{2}H/^{1}H$) and oxygen ($^{18}O/^{16}O$) in natural waters vary throughout the water cycle as a result of hydrological processes, such as evaporation, condensation, and mixing (e.g. Clark & Fritz, 1997). For the Breckenridge site, these isotope ratios can provide insight into the different potential source waters: meteoric water (precipitation), glacial meltwater, and seawater. In environments with low permeability thick clay deposits, such as in the Breckenridge borehole, stable isotopes can sometimes be used to quantify groundwater flow and diffusion (Desaulniers et al., 1981; Desaulniers and Cherry, 1989), in addition to processes which also affect the concentrations of other ions (e.g. $Na^{+}$, $Ca^{2+}$) relevant to the geotechnical properties of Champlain Sea sediments. Isotope ratios are reported as permil (‰, parts per thousand) differences (δ) relative to Vienna standard mean ocean water (VSMOW), the standard reference for $^{18}O$ and $^{2}H$ measurements.

In 2014, pore water from each core segment was analysed for $\delta^{2}H$ and $\delta^{18}O$ at EIL (University of Waterloo) by a Los Gatos Research – Off-Axis Integrated Cavity Output Spectroscopy (LGR-OA-ICOS) laser system. The LGR "EP LWIA" instrument has precisions of: $\delta^{2}H=\pm0.3‰$ and $\delta^{18}O=\pm0.1‰$. EIL quotes precisions of: $\delta^{2}H=\pm0.8‰$ and $\delta^{18}O=\pm0.2‰$. Approximately 1000 nL of pore water was injected into the heated septum port by a LEAP Technology™ (CTC) PAL liquid auto-sampler. Upon injection, the water rapidly vaporized and was expanded into the laser cell of the EP LWIA. Unlike mass spectrometry techniques, the $H_2O$ molecules were not converted to other gases, but rather were measured directly by the ICOS Laser System. All samples were pre-filtered to 0.45 μm. The instrumental analysis was recommended by the International Atomic Energy Agency for isotopic analysis in water. The instruments have been in use for approximately 10 years; EIL used the 2013 model. Limits of the analysis are: conductivity <5000 μS/cm, TDS <500mg/L, pH 5 to 9, and not coloured and/or odorous (because of volatile organic compounds (VOCs)). Although limits for conductivity and TDS were exceeded by the high-salinity intervals of the Breckenridge drill core, precision and accuracy of the measurements were not compromised. However, higher conductivity and TDS can lead to a more rapid rate of salt accumulation in the analytical instrument and can generate mechanical system failures (Heemskerk, pers. comm., 2016).

Results, presented in Figure 17, indicate that $\delta^{18}O$ and $\delta^{2}H$ values from Breckenridge pore waters plot along the global meteoric water line. The shallowest sample (sample 3, depth 2.83 m) has a similar isotopic composition to that of modern average Ottawa precipitation which is consistent with the introduction of modern meteoric waters through shallow fractures caused by desiccation cracking. However, deeper samples are more enriched, indicating the mixing of fresh water and seawater in the Champlain Sea at the time of sediment deposition. The geochemical, hydrogeological, and geotechnical implications of these results are topics of ongoing research.

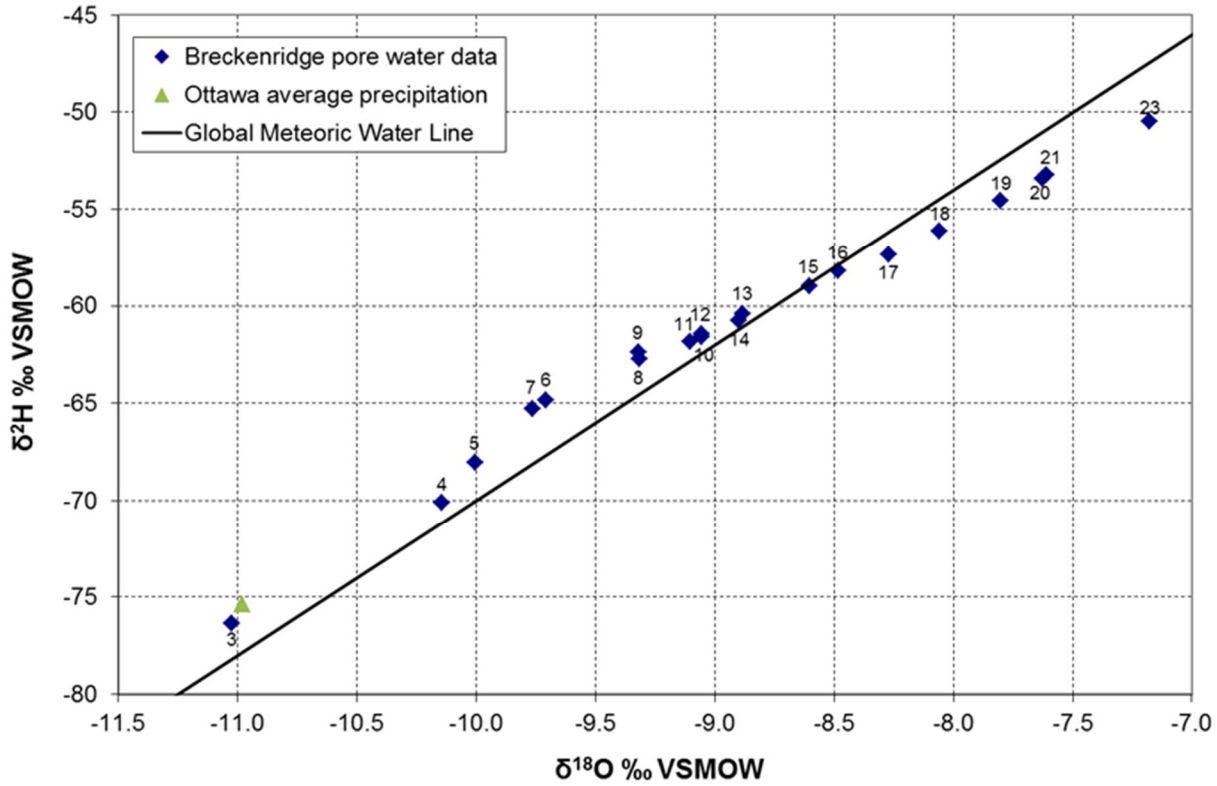


**Figure 17**. $\delta^{2}H$ versus $\delta^{18}O$ of Breckenridge pore waters. Ottawa average precipitation from IAEA (2016). Labels indicate core segment numbers.

### 3.3 Mineralogy studies

The lab techniques used for the mineral identification studies of five samples are summarized below. Additional figures containing SEM-EDS spectra are provided in Appendix B-2.

#### 3.3.1 X-ray diffraction analysis

Five samples were selected for XRD analyses: two samples from sand seams near the base of the borehole, and three silt samples from the top, middle, and bottom of the borehole (Table 9). Both pressed powder and smear mounts were prepared. Bulk samples were pulverized using a McCrone micronizing mill in isopropyl alcohol for 5 minutes to obtain a grain size of about 5 - 10 µm. The samples were dried and then back pressed into an aluminum holder to produce a randomly oriented specimen. For smear mounts, 40 mg were suspended in distilled water, pipetted onto glass slides, and air-dried overnight to produce oriented mounts. X-ray patterns of the pressed powders or air-dried samples were recorded on a Bruker D8 Advance Powder Diffractometer equipped with a Lynx-Eye Detector, Co Kα radiation set at 40 kV and 40 mA. The smear mounts were also X-rayed following saturation with ethylene glycol and heat treatment.

Initial identification of minerals was made using EVA (Bruker AXS Inc.) software with comparison to reference mineral patterns using Powder Diffraction Files (PDF) of the International Centre for Diffraction Data (ICDD) and other available databases. Quantitative analysis by Rietveld refinement was carried out using TOPAS (Bruker AXS Inc.).

Results (wt%) from the quantitative (pressed powder) and semi-quantitative (smears) are provided in Table 9, and reflect a material largely derived from the Precambrian Shield. The pressed powder or bulk sample results show they are dominated by plagioclase feldspar and quartz with subordinate K-feldspar, amphibole and biotite. Clinopyroxene and chlorite occur in minor amounts, and calcite, fluorapatite, and pyrite in trace amounts. The semi-quantitative results for the smears are comparable in relative proportions to the pressed powder samples, and show no evidence of smectite or mixed-layer clay minerals. The Goodness of Fit (GoF) is low to moderate indicating a good match to the reference mineral structures. These results are comparable to those reported in Percival et al. (2001) examining the mineralogy of coloured rhythmites from selected boreholes in the vicinity of the Lemieux, Ontario landslide.

A sample XRD profile is shown in Figure 18 for a sample taken from core segment 21. The top shows the results for the smear sample and no changes occur with the treatments, indicating an absence of mixed-layer clay minerals or smectite. The bottom illustrates the Rietveld refinement analysis for the pressed powder sample. Note that the mineral species selected are the best fit but do not necessarily indicate the true chemical composition of the mineral in the sample.

**Table 9.** Mineralogy (wt%) of samples selected from the Champlain Sea sediments near Breckenridge, QC using two methods: pressed powders and smear mounts.

| Core Segment | Depth (Top) | Depth (Bot) | Qtz | Pl | Kfs | Amp | Cpx | Bt | Chl | Cal | FAp | Py | GoF |
|---|---|---|---|---|---|---|---|---|---|---|---|---|---|
| **Quantitative mineralogy (wt%) of bulk (pressed powder) samples** | | | | | | | | | | | | | |
| 05 | 8.40 | 8.92 | 16 | 32 | 12 | 12 | 4 | 17 | 7 | tr | | | 3.25 |
| 13 | 32.40 | 33.01 | 16 | 36 | 11 | 12 | 2 | 18 | 5 | tr | | | 2.1 |
| 21 | 59.61 (sand seam) | | 31 | 40 | 12 | 9 | 2 | 6 | tr | tr | tr | tr | 3.59 |
| 22 | 62.40 | 62.45 | 19 | 39 | 11 | 12 | 3 | 15 | 1 | tr | | | 2.44 |
| 23 | 64.16 (sand seam) | | 30 | 41 | 12 | 11 | 3 | 2 | 1 | tr | tr | tr | 2.86 |
| **Semi-quantitative mineralogy (wt%) of smear mount samples** | | | | | | | | | | | | | |
| 05 | 8.40 | 8.92 | 15 | 32 | 11 | 12 | 3 | 20 | 7 | tr | | | 2.19 |
| 13 | 32.40 | 33.01 | 14 | 35 | 12 | 15 | 3 | 17 | 4 | tr | | | 2.38 |
| 21 | 59.61 (sand seam) | | 26 | 39 | 12 | 10 | 3 | 10 | tr | tr | tr | tr | 2.16 |
| 22 | 62.40 | 62.40 | 15 | 37 | 10 | 13 | 3 | 18 | 4 | | tr | tr | 2.52 |
| 23 | 64.14 (sand seam) | | 29 | 41 | 12 | 11 | 3 | 2 | 2 | tr | tr | tr | 2.19 |

Qtz: quartz; Pl; plagioclase; Kfs: K-feldspar; Amp: amphibole; Cpx: clinopyroxene; Bt: biotite; Chl: chlorite; Cal: Calcite; FAp: fluorapatite; Py: pyrite; tr: trace; GoF: goodness of fit.

### 3.3.2 Scanning electron microscopy

To verify the presence of particular minerals, SEM analyses were also performed on grain mounts of sand samples 21 and 23. A Zeiss EVO 50 series Scanning Electron Microscope with Extended Pressure capability (up to 3000 Pascals) was used for these analyses, with a Backscattered Electron Detector (BSD), an Everhart - Thornley Secondary Electron Detector (SE), a Variable Pressure Secondary Electron Detector (VPSE), and a Cathodoluminescence Detector (CL).

Based on SEM analyses, the presence of apatite, amphibole, and clinopyroxene detected in samples from cores 21 and 23 by XRD was confirmed. Energy dispersive spectra (EDS) from each of these minerals can be found in Appendix B-2. In addition, trace amounts of magnetite, ilmenite, zircon, titanite, monazite, and allanite were observed. Fluorapatite was identified, and the mica present was verified to be biotitic. The presence of magnetic minerals (magnetite and ilmenite), even in trace amounts, are reflected in the increase of the downhole magnetic susceptibility log in the presence of sand (see Figure 9 and log in Appendix A-3).

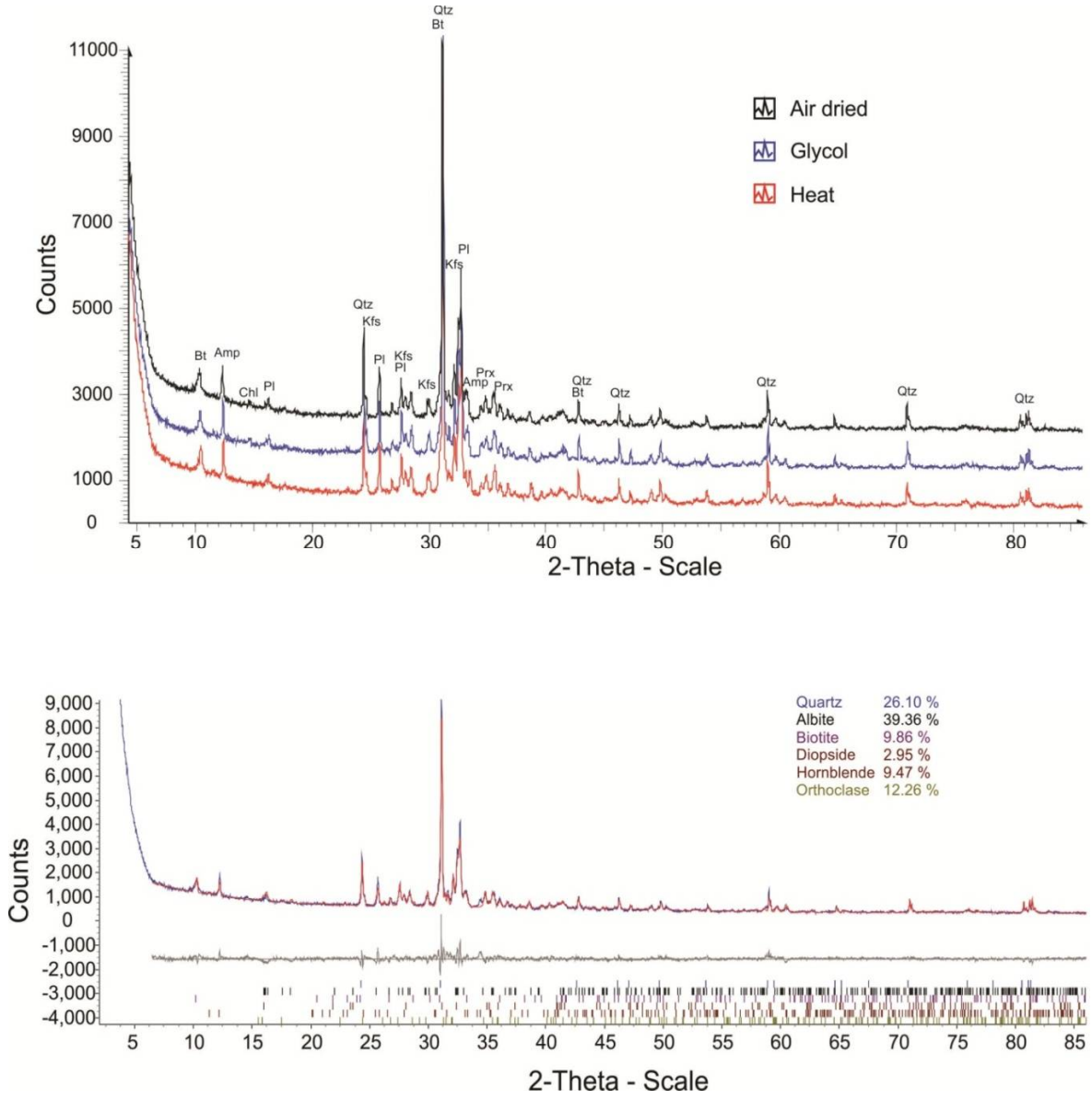


**Figure 18.** XRD profile of a sample taken from core segment 21 (sand seam) prepared as a smear mount. Top – Initial analysis done on an air dried, glycol-saturated and heat-treated sample, processed using EVA software. Bottom - Rietveld refinement method applied to a pressed powder sample for quantitative mineral analysis using TOPAS software. Residual pattern shown in grey. Albite, diopside, hornblende and orthoclase are the best matches for this sample.

### 3.3.3 Portable X-Ray fluorescence (pXRF) spectrometry

Portable X-ray fluorescence (pXRF) spectrometry is a cost effective, non-destructive tool that can be used to provide chemostratigraphic data that is often beyond the budget of most soil studies. Reliability of this method was documented by Knight et al. (2013) by comparing pXRF results with fusion chemistry (ICP-ES/MS) of fine-grained Champlain Sea sediments collected from a GSC borehole located near Kinburn, Ontario, 23 km west of the Breckenridge borehole.

For the Breckenridge study, 20 sediment samples from the core segments were freeze-dried, disaggregated, sieved to <0.063 mm, and placed in plastic vials sealed with 6 micron thick SpectroCertified Mylar® polyester prior to pXRF analysis. The fine sand/silt/clay powders were analyzed using a handheld Thermo Scientific, Niton XL3t GOLDD XRF spectrometer by placing the sample in a test stand with the Mylar® in contact with the analyzer. The pXRF analyzer is equipped with a 50-kV X-ray tube. Samples were analyzed in soil mode for trace elements occurring with expected concentrations of <1%. For each analysis a dwell time of sixty seconds was used for high, main, and low filters for a total dwell time of three minutes per analysis. Elements, detected by each filter and the corresponding lower limits of detection, as provided by NITON, are listed in Table 10. For calibration, standard samples of Till-4, Resource Conservation and Recovery Act (RCRA), NCS 73308, and a $SiO_2$ blank were analyzed at the beginning and end of each analytical session and at an interval of every 10 samples.

From the pXRF, fifteen elements (As, Ba, Ca, Cr, Cu, Fe, K, Mn, Rb, Sr, Ti, V, Zn, and Zr) were present in sufficient quantities to be detected (Table 10). Elements below detection limit or with known reliability concerns (such as Sc) have been removed from the summary data set.

Data obtained by pXRF spectrometry were plotted with respect to depth to visualize the chemostratigraphy of the borehole, and to highlight downhole trends in elemental concentrations (see Appendix B-3). Results are in agreement with the concentrations measured in a well-studied Champlain Sea sediment borehole (97 m in depth) drilled by the GSC in Kinburn, ON (Knight et al., 2012). Variations in the chemostratigraphy are subtle in these fine grained sediments, however, when combined with downhole geophysical logs, grain size data, and core logging observations, information from all data sets may provide insight into changes in depositional conditions.

**Table 10**. Elements detected in the Breckenridge borehole and corresponding detection limits (ppm) for pXRF using two matrix configurations and filters.

| Element | Matrix | | Filter |
|---|---|---|---|
| | $SiO_2$ | $SiO_2$ + Fe +Ca | |
| As | 4 | 7 | High |
| Ba | 35 | 45 | Low |
| Ca | 40 | N/A | Low |
| Cr | 10 | 22 | Main |
| Cu | 10 | 13 | Low |
| Fe | 25 | N/A | Main |
| K | 45 | 150 | Low |
| Mn | 35 | 50 | Main |
| Rb | 3 | 3 | Main |
| Sr | 3 | 3 | Low |
| Ti | 20 | 60 | Low |
| V | 10 | 25 | Low |
| Zn | 7 | 10 | Main |
| Zr | 3 | 4 | Main |

### 3.4. Mollusc shell fragment identification and radiocarbon date

The purpose of this aspect of the study was to estimate time constraints on sediment deposition in the Champlain Sea at the Breckenridge borehole location and to infer the environmental conditions at the time of deposition (e.g., water depth, salinity range). Some insights can be gleaned from identifying and analysing a bivalve fragment (Figure 19), which was encountered in core segment 19 (see Figure 9 for shell depth within the sediment column).

The mollusc fragment was removed from the sediments when the core was extruded (14 April 2014) and stored in a sealed clear plastic vial until identification and analysis in March 2017. Its weight was 14.1 mg. Dimensions were approximately 5 mm × 5 mm. It represents the only datable material within the retrieved cores. Figure 19 shows both external and internal views of the bivalve fragment.

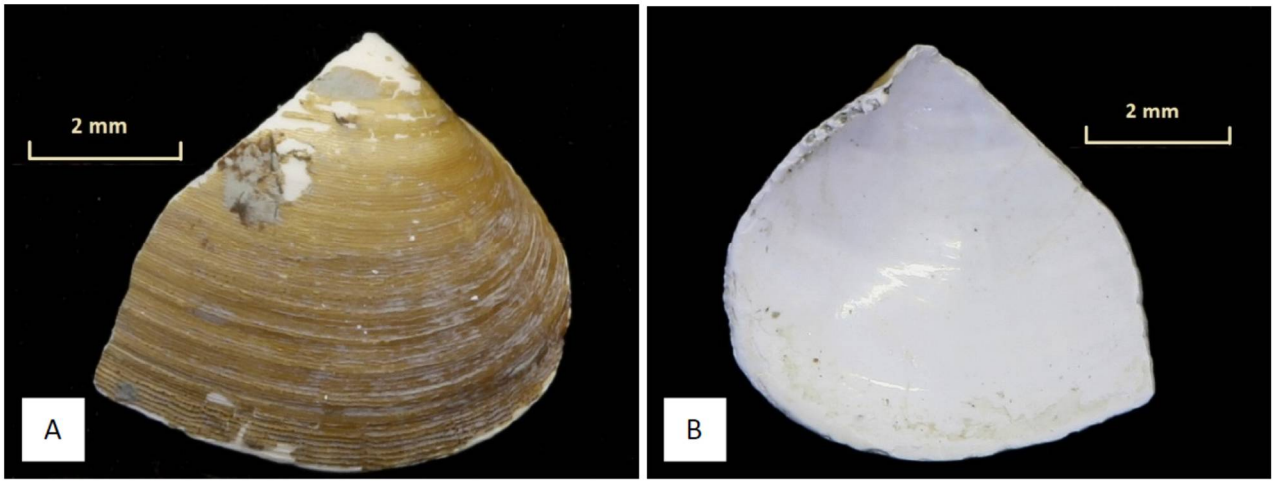


**Figure 19.** Images of bivalve fragment. (A) external view and (B) internal view.

#### 3.4.1. Identification

Observations of the specimen include its relatively small size and fine growth lines evident on the exterior view (Figure 19A; M. Cournoyer, pers. comm., 2017). The umbo (apex or highest point of the shell) is near the anterior edge of the valve; this is deduced by the growth lines that continue in straight lines towards the posterior (i.e., the broken portion). The perostracum (exterior skin layer) is preserved (Figure 19A). The specimen was not found in abundance, as it was the only substantial fossil fragment discovered in the core. Teeth are present on the interior of the valve near the umbo (Figure 19B). Although a dorsal view is not shown, the specimen had a curvature and did not exhibit a flat profile.

From these observations and by comparing attributes with those of known specimens (Costello *et al.*, 2001), it is likely that the bivalve fragment is a member of the *Portlandia* genus, possibly a juvenile of the species *Portlandia arctica* (Huber & Gofas, 2010), as deduced by the Musée de paléontologie et de l'évolution in Montreal (M. Cournoyer, pers. comm., 2017). Its relatively small size suggests that the specimen is a juvenile. Although preservation of the perostracum is unusual, it has been observed in fossils of this species. The lack of abundance of fossils in the core is consistent with *Portlandia*, which is usually found isolated. Its low abundance, combined with its curvature (i.e., not flat along the sagittal plane), also suggests that it belongs to

the *Portlandia* genus and not *Macoma*, which is flat and observed in abundant numbers (M. Cournoyer, pers. comm., 2017).

### 3.4.2. Depositional and ecological environment

Of particular note, *Portlandia arctica* is a deposit feeder (Bernard, 1979), which can survive in environments with low organic carbon content and rapid sedimentation rates (Cai, 2006). It has been identified as an ice-proximal aggressive colonizer in under-consolidated mud and sand and is viewed as a biomarker for glacio-marine facies development during early glacial retreat (e.g., Giangioppi, 2003; Hillaire-Marcel, 1980; Occhietti *et al.*, 2001). It appears typically at the base of the marine sequence. *Portlandia arctica* has been characterized as relatively stenohaline (Giangioppi, 2003) with a minimum salinity of 23 (Peacock, 1993), although it is known to tolerate dilution by meltwater. Salinity ranges have been estimated to be on the order of 10-34 (Cummings *et al.*, 2011 and references therein; Giangioppi, 2003). The calculated salinity for core segment 19, from which the *Portlandia* fragment was obtained, is 17.9 (on the Practical Salinity Scale-78), based on the chloride concentration measured in the extracted pore water.

*Portlandia* is a well-known component of Champlain Sea sediments (e.g., Cronin, 1979) and is observed: (1) isolated in low abundances; (2) as a juvenile (Naldrett, 1988); (3) in low-diversity environments (Hillaire-Marcel, 1980); and (4) with other fossil remains, not necessarily in the same stratigraphic interval (e.g., other deposit feeders (*Macoma*), suspension feeders (*Hiatella arctica*), foraminifera (Hillaire-Marcel, 1980; Cronin, 1977; 1988), ostracodes (Cronin, 1988) and mammals (e.g., whales; Harington, 1977; Cummings *et al.*, 2011, and references therein; Rodrigues & Richard, 1986). When its occurrence was observed as a juvenile and in fragments, its depositional environment was interpreted to be too harsh for survival to adult forms with high mortality rates (Naldrett, 1988). In the Champlain Sea, *Portlandia* likely occurs in cold ($\leq 0$°C) ice-proximal waters greater than 30 m deep (Cronin, 1979), although it has been observed at higher Arctic latitudes in water depths interpreted to be 4–81 m (Cai, 2006) and 10–400 m (Gaingioppi, 2003).

### 3.4.3. Radiocarbon dating - Accelerator Mass Spectrometer (AMS)

Radiocarbon dating yields a measurement of the ratio of radiocarbon to stable carbon in the mollusc fragment. The ratio of radiocarbon to stable carbon decreases as the unstable radiocarbon atoms decay with time, from which the organism's age in radiocarbon years can be calculated. The method is applicable for ages up to about 50,000 years; for older samples, the radiocarbon content would be below detection. Calibration is a necessary step to correct for atmospheric fluctuations in decay rates or in the ratio of historic radiocarbon to stable carbon. A light acid etch (acid-base-acid; HCl-NaOH-HCl wash) was used as a chemical pre-treatment to remove approximately 20% of the exterior film on the mollusc fragment (Crann *et al.*, 2016) with apparatus described by St-Jean *et al.* (2016). Between the light etch and combustion required for graphitization (to yield elemental carbon), the specimen was consumed in its entirety for processing and radiocarbon analysis. Data reporting conventions followed recommendations of Millard (2014).

A 3-megavolt (MV) tandem AMS (High Voltage Engineering) was used for radiocarbon analysis at the André E. Lalonde AMS Laboratory, University of Ottawa. The $^{12,13,14}C^{+3}$ ions were measured at 2.5 MV terminal voltage with Ar stripping. The fraction of modern carbon, $F^{14}C$, was calculated as the ratio of $^{14}C/^{12}C$ in the sample to $^{14}C/^{12}C$ in the standard (Ox-II) measured in the same run and according to Reimer *et al.* (2013). The two $^{14}C/^{12}C$ values were background-corrected and the result corrected for spectrometer and preparation fractionation using the measured $^{13}C/^{12}C$ value normalized to $\delta^{13}C$ (PDB). Radiocarbon ages were calculated as

–8033(ln($F^{14}C$)) and reported in $^{14}C$ yr BP (before present; BP=AD 1950) as described by Stuiver & Polach (1977). Errors in $^{14}C$ ages (1σ) were calculated from counting statistics and variations of $^{14}C/^{12}C$ and $^{13}C/^{12}C$ between analytical runs. Although customary to report radiocarbon data with $\delta^{13}C$ content, in this instance it was not reported because $\delta^{13}C$ was measured internally by the AMS and accounts for isotopic fractionation within the instrument.

Unlike Arctic Canada (Coulthard *et al.*, 2010), the regional difference from the average global marine reservoir correction (ΔR) was not applied to the sample results, as there were no records in the immediate vicinity (CHRONO database; http://calib.org/marine/ accessed 12 May 2017). Since the Champlain Sea had inundated so far inland to the west, the closest records, nearly 400 km to the east, were likely not relevant (Quebec City; S. Murseli, pers. comm., 2017). However, results were calibrated with OxCal v.4.2.4 (Bronk Ramsay, 2009) and the Marine13 calibration curve, a global marine correction to account for the longer residence time of carbon in the ocean (Reimer *et al.*, 2013).

AMS dating yielded a radiocarbon age of 11486 ± 38 $^{14}C$ yr BP (lab ID UOC-3809). The calibrated age range is 13096-12801 cal BP ($F^{14}C$ = 0.2394 ± 0.0011). The AMS date of the *Portlandia* specimen from the Breckenridge borehole lies within the reported dates of other *Portlandia* species at different locations within Champlain Sea sediments (LaSalle, 1966; Hillaire-Marcel, 1974; Occhietti, 1976; Rodrigues, 1992; LaSalle & Shilts, 1993; McNeely & Jorgensen, 1993). It is also consistent with reported radiocarbon ages of the Champlain Sea (12.5 to 10.0 ka BP (Corliss *et al.*,1982); 11.4-11.6 ka BP (Rodrigues, 1992); 11.1 ka BP, from pollen (Richard & Occhietti, 2005)).

Because the genus *Portlandia* is a deposit-feeding mollusc, it likely incorporates other carbon sources not in equilibrium with ambient seawater, such as organic matter (e.g., Forman & Polyak, 1997; Mangerud *et al.*,2006) or dissolved carbonate from sediment pore water (Dyke, 2004). This mixing of contemporaneous seawater carbon during the life of the mollusc with other carbon sources yields an older or exaggerated radiocarbon age (England *et al.*, 2013). In the Breckenridge borehole, there were no suspension feeders encountered to compare radiocarbon ages. Therefore the radiocarbon age of the broken *Portlandia* fragment may serve as a conservative age limit or constraint for the time of its deposition in the sediments at 53.40-53.98 m depth.

## 4.0 Summary

The purpose of this report was to document the many data sets resulting from multidisciplinary investigations of Champlain Sea sediments at a test site in western Quebec. Paleolandslides and amplified shaking have resulted from earthquakes in this region, and these data sets will form a needed base for further ground motion research at this site. The data sets, at both large and small scales, provide context for the depositional and temporal changes in conditions which are affecting the geotechnical behaviours of the sediments.

Ongoing research will use the new data sets presented herein to investigate:

- the processes through which pore waters at this site may have been leached, and the use of surficial geophysical techniques to identify soils which may be prone to retrogressive behaviour once slope failure is triggered;
- the variation in sediment mineralogy (thus provenance) at the site, and the role of XRD, pXRF, and downhole geophysical logging techniques in detecting subtle mineralogical changes in Champlain Sea sediments; and
- seismograph monitoring on closely spaced soil and rock sites and 2D ground motion modeling to further study the complex effects of amplification in soft soil-filled basins, a common feature in eastern Canada.

## 5.0 Acknowledgments

The authors gratefully acknowledge the permission of Mr. Bob Brizzard for access to his land and his continued support to conduct field investigations over many years. Thanks to George Downing Estate Drilling Ltd. who conducted the drilling at the site.

From the GSC, we thank: Kevin Brewer and Tim Cartwright for their work on site during the field geophysical surveys and drilling; Claudia Moore for her careful work on pore water extraction and for imaging the mollusc; Michelle Coyne for her assistance in securing paleontological expertise; and Matt Pyne for cartography support. Thanks to Dr. Greg Brooks for his review of this report, and for the collection of numerous microtremor recordings in remote locations across the study area. Thanks also to Dr. Didier Perret for feedback and discussion on the geophysical and geotechnical data sets.

We acknowledge expertise which came from outside the GSC. With thanks to: Richard Heemskerk and laboratory personnel at EIL (University of Waterloo) for direct isotopic analyses of pore water; M. Cournoyer for expert identification of the mollusc fragment (Musée de paléontologie et de l'évolution, Montreal); S. Murseli, X-L Zhao, and W. E. Kieser (University of Ottawa) for radiocarbon age dating at the André E. Lalonde AMS Laboratory (University of Ottawa).

We acknowledge the work of dedicated students who assisted in data collection at the site and analyses of data and cores over many years, including: Jessie Duguay-Blanchette (Univ. Laval), Andrea Reman (Univ. Waterloo), Sara McPeak and Amin Esmaeilzadeh (Carleton Univ.), and Matthew Griffiths (Univ. Victoria).

The geotechnical characterization of the cores from GSC-BH-BRK-01 and -02 was conducted by Jessie Duguay-Blanchette with support from NSERC Grant RDCPJ 444172-12. Funding of this project was provided through the GSC's Public Safety Geoscience Program.

## 6.0 References

ASTM D4220 / D4220M-14, Standard Practices for Preserving and Transporting Soil Samples, ASTM International, West Conshohocken, PA, 2014, www.astm.org

ASTM D4318-10e1, Standard Test Methods for Liquid Limit, Plastic Limit, and Plasticity Index of Soils, ASTM International, West Conshohocken, PA, 2010, www.astm.org

Bélanger R, 2008. Urban geology of the National Capital area / Géologie urbaine de la région de la Capitale nationale; Geological Survey of Canada, Open File 5311, 2008; 1 DVD, doi:10.4095/226165

Bernard F R, 1979. Bivalve mollusks of the Western Beaufort Sea. Contributions in Science, Natural History Museum of Los Angeles County 313, 80 pp.

Brooks G R, 2013. A massive sensitive clay landslide, Quyon Valley, southwestern Quebec, Canada, and evidence for a paleoearthquake triggering mechanism; Quaternary Research (New York) vol. 80, no. 3, 2013; p. 425-434, doi:10.1016/j.yqres.2013.07.008

Brooks G R, Medioli B E, Aylsworth J M, Lawrence D E, 2013. A compilation of radiocarbon dates relating to the age of sensitive clay landslides in the Ottawa Valley, Ontario-Québec; Geological Survey of Canada, Open File 7432, 62 pages, doi:10.4095/292913 http://ftp.maps.canada.ca/pub/nrcan_rncan/publications/ess_sst/292/292913/of_7432.pdf [accessed: Mar 2017]

Bronk Ramsey C, 2009. Bayesian analysis of radiocarbon dates. Radiocarbon 51: 337–360.

Budhu M, 2007. Soil mechanics and foundations, Wiley, 634 p.

Cai S, 2006. Paleoenvironmental interpretation of late glacial and post-glacial fossil marine molluscs, Eureka Sound, Canadian arctic archipelago. MSc Thesis, University of Saskatchewan. 161 pp.

Casagrande A, 1932. Research on the Atterberg limits of soil. Public Roads 13(8): 121-136.

CFEM, 2006. Canadian Foundation Engineering Manual, 4th Edition, Canadian Geotechnical Society, BiTech Publishers, 488p.

CAN/BNQ 2501-170/2014, 2014. Soils – Determination of water content, National Standard of Canada / Bureau de Normalization du Quebec, www.bnq.qc.ca

CAN/BNQ 2501-092/2014, 2014. Soils – Determination of liquid limit by a fall cone penetrometer and determination of plastic limit, National Standard of Canada / Bureau de Normalization du Quebec, www.bnq.qc.ca

Clark I, Fritz P, 1997. Environmental Isotopes in Hydrogeology. CRC Press LLC, Boca Raton, pp. 328.

Corliss B H, Hunt A S, Keigwin L D Jr, 1982. Benthonic foraminiferal faunal and isotopic data for the postglacial evolution of the Champlain Sea. Quaternary Research 17: 325-338.

Costello M J, Emblow C S, White R (ED), 2001. European Register of Marine Species. A check-list of the marine species in Europe and a bibliography of guides to their identification. *Patrimoines naturels* 50: 463 p.

Coulthard R D, Furze M F A, Pieńkowski A J, Nixon F C, England, J H, 2010. Quaternary Geology 5: 419-434.

Crann C, Murseli S, St-Jean G, Zhao X, Clark I, Kieser W, 2016. First Status Report on Radiocarbon Sample Preparation Techniques at the A.E. Lalonde AMS Laboratory (Ottawa, Canada). Radiocarbon 1-10. doi:10.1017/RDC.2016.55

Crawford C B, Eden W J, 1967. Stability of natural slopes in sensitive clay, in Proceedings of the American Society of Civil Engineers, 93**,** SM4, pp. 419436.

Cronin T M, 1977. Champlain Sea foraminifera and ostracoda: A systematic and paleoecological synthesis. Géographie Physique et Quaternaire 31(1/2): 107-122.

Cronin T M, 1979. Late Pleistocene benthic foraminifers from the St. Lawrence lowlands. Journal of Paleontology 53(4): 781-814.

Cronin T M, 1988. Paleozoogeography of postglacial ostracoda from Northeastern North America. IN: The Late Quaternary development of the Champlain Sea basin. ED: Gadd, N.R. Geological Association of Canada special paper 35: 125-144.

Crow H, LeBoeuf D, Sivathayalan S, Motazedian D, Cascante G, 2013. Investigating the Dynamic Properties of Leda Clay, in proceedings, Eastern Section of the Seismological Society of America, LaMalbaie, QC. [abstract]

Crow H, Good R L, Hunter J A, Burns R A, Reman A, Russell H A J, 2015. Borehole geophysical logs in unconsolidated sediments across Canada; Geological Survey of Canada, Open File 7591; 39 pages, doi:10.4095/295753
http://ftp.maps.canada.ca/pub/nrcan_rncan/publications/ess_sst/295/295753/of_7591.zip [accessed: Mar 2016]

Cummings D I, Gorrell G, Builbault, J-P, Hunter J A, Logan, C, Ponomarneko D, Pugin, A J-M, Pullan S E, Russell H A J, Sharpe D R, 2011. Sequence stratigraphy of a glaciated basin fill, with a focus on esker sedimentation. GSA Bulletin. 123 (7/8): 1478-1496; doi: 10.1130/B30273.1; 15 figures.

Desaulniers D E, Cherry J A, Fritz P, 1981. Origin, age and movement of pore water in argillaceous Quaternary deposits at four sites in southwestern Ontario. Journal of Hydrology, 50(C): 231-257.

Desaulniers D E, Cherry J A, 1989. Origin and movement of groundwater and major ions in a thick deposit of Champlain Sea clay near Montreal. Canadian Geotechnical Journal, 26(1): 80-89.

Duguay-Blanchette, J, 2016. Étude du comportement statique et cyclique de deux argiles sensibles de l'est du Canada. Master's thesis, Université Laval, Québec, Canada, 254p.
http://theses.ulaval.ca/archimede/meta/31643 [accessed: Feb 2017]

Dyke A S, 2004. An outline of North American deglaciation with emphasis on central and northern Canada. IN: Developments in Quaternary Sciences 2 (Part B): 373-424.

Eden W J, Mitchell R J. 1970. The mechanics of landslides in Leda Clay, Canadian Geotechnical Journal, 7, 285 - 296.

England J, Dyke A S, Coulthard R D, McNeely R, Aitken A, 2013. The exaggerated radiocarbon age of deposit-feeding molluscs in calcareous sediments. Boreas 42: 362-373.

Farquharson C G, Oldenburg D W, 1998. Non-linear inversion using general measures of data misfit and model structure. Geophysical Journal International 134, 213–227.

Forman S L, Polyak L, 1997. Radiocarbon content of pre-bomb marine mollusks and variations in the $^{14}C$ reservoir age for coastal areas of the Barents and Kara seas, Russia. Geophysical Research Letters 24: 885–888.

Garneau R, LeBihan P, 1977. Estimation of some properties of Champlain clays with the Swedish fall cone. Canadian Geotechnical Journal, 14, 571-581.

Geonics, 2006. EM39 – Borehole Conductivity Logger Operating Manual, Geonics Limited, Mississauga, ON.

Giangioppi M, Little E C, Ferbey T, Ozyer C.A, Utting D J, 2003. Quaternary glaciomarine environments west of Committee Bay, central mainland Nunavut. Geological Survey of Canada, Current Research 2003-C5, 12 p.

Gouvernement du Québec, 2016. Produits dérivés de base LiDAR; https://www.donneesquebec.ca/recherche/fr/dataset/produits-derives-de-base-du-lidar [accessed: Mar 2017)

Halchuk S. 2010. Intensity reports for the Val-des-Bois, Québec, earthquake of June 23, 2010; Canadian Hazard Information Service Internal Report 2010-3.1; 15 pages, doi:10.4095/287438 http://ftp.maps.canada.ca/pub/nrcan_rncan/publications/ess_sst/287/287438/chis_ir_2010_3_1.zip [accessed: Mar 2017]

Hansbo S. 1957. A new approach to the determination of the shear strength of clay by the fall cone test. In proceedings: Royal Swedish Geotechnical Institute, Stockholm, No. 14

Harington C R, 1977. Marine mammals in the Champlain Sea and the Great Lakes. Annals of the New York Academy of Sciences 288(1): 508-537.

Hillaire-Marcel C, 1974. La déglaciation au Nord-Ouest de Montréal: Données radiochronologiques et faits stratigraphiques. Rev. Géogr. Montreal 28(4): 407-417

Hillaire-Marcel C, 1980. Les faunes des mers post-glaciaires du Québec: quelques considérations paléoécologiques. Géographie physique et Quaternaire, 34 (1): 3-59.

Huber M, Gofas S, 2010. *Portlandia arctica* (Gray, 1824). IN: MolluscaBase (2017). Accessed at http://www.molluscabase.org/aphia.php?p=taxdetails&id=141987 on 2017-05-17

Hunter J A, Burns R A, Good R L, Pullan S E, Harris J B, Skvortzov A, Goriainov N N, 1998, Downhole seismic logging for high-resolution reflection surveying in unconsolidated overburden; Geophysics, Vol 63, No. 4, pp. 1371-1384.

Hunter J A, Crow H L (eds.), 2015. Shear wave velocity measurement guidelines for Canadian seismic site characterization in soil and rock; Earth Sciences Sector, General Information Product 110; 226 pages, doi:10.4095/297314 http://ftp.maps.canada.ca/pub/nrcan_rncan/publications/ess_sst/297/297314/gip_110_e.zip [accessed: Mar 2017]

Hunter J A, Crow H L, Brooks G R, Pyne M, Motazedian D, Lamontagne M, Pugin A J-M, Pullan S E, Cartwright T, Douma M, Burns R A, Good R L, Kaheshi-Banab K, Caron R, Kolaj M, Folahan I, Dixon L, Dion K, Duxbury A, Landriault A, Ter-Emmanuil V, Jones A, Plastow G. and Muir D, 2010. Seismic Site Classification and Site Period Mapping in the Ottawa Area Using Geophysical Methods; Geological Survey of Canada, Open File 6273, 1 DVD. http://ftp.maps.canada.ca/pub/nrcan_rncan/publications/ess_sst/286/286323/of_6273.zip [accessed: Mar 2017]

IAEA/WMO, 2016. Global Network of Isotopes in Precipitation. The GNIP Database. Accessible at: http://www.iaea.org/water.

Khaheshi Banab K, Kolaj M, Motazedian D, Sivathayalan S, Hunter J A, Crow H L, Pugin A J-M, Brooks G, 2012. Seismic Site Analysis for Ottawa, Canada: A Comprehensive Study Using Measurements and Numerical Simulations; Bulletin of the Seismological Society of America, Vol. 102, No. 5, pp. 1976–1993, October 2012, doi: 10.1785/0120110248

Knight R D, Moroz M, Russell H A J, 2012. Geochemistry of a Champlain Sea aquitard, Kinburn, Ontario: portable XRF analysis and fusion chemistry; Geological Survey of Canada, Open File 7085; 28 pages, doi:10.4095/290969
http://ftp.maps.canada.ca/pub/nrcan_rncan/publications/ess_sst/290/290969/of_7085.zip [accessed: Mar 2016]

Knight R D, Kjarsgaard B A, Plourde A P, Moroz M, 2013. Portable XRF spectrometry of reference materials with respect to precision, accuracy, instrument drift, dwell time optimization, and calibration; Geological Survey of Canada, Open File 7358; 45 pages, doi:10.4095/292677
http://ftp.maps.canada.ca/pub/nrcan_rncan/publications/ess_sst/292/292677/of_7358.zip [accessed: Mar 2016]

Kramer S L, 1996. Geotechnical Earthquake Engineering, Prentice Hall, 653 p.

LaSalle P, 1966. Late Quaternary vegetation and glacial history in the St. Lawrence lowlands. Leidre Geol. Medel. 38: 1-128.

LaSalle P, Shilts W W, 1993. Younger Dryas-age readvance of Laurentide ice into the Champlain Sea. Boreas, 22: 25-37.

Lewis E L, 1980. The Practical Salinity Scale 1978 and its antecedents. IEEE Journal of Oceanic Engineering, 5(1): 3-8.

Lewis E.L, Perkin R G, 1981. The practical salinity scale 1978: conversion of existing data. Deep Sea Research Part A, Oceanographic Research Papers, 28(4): 307-328.

L'Heureux J-S, Locat A, Leroueil S, Demers D, Locat J (eds.), 2014 Landslides in Sensitive Clays: From Geosciences 1 to Risk Management, Advances in Natural and Technological Hazards Research 36, DOI 10.1007/978-94-007-7079-9_1, Springer Science+Business Media Dordrecht

Loke M H, Acworth I, and Dahlin T, 2003. A comparison of smooth and blocky inversion methods in 2D electrical imaging surveys. Exploration Geophysics 34, 182–187.

Loke M H, Chambers J E, Rucker D F, Kuras O, Wilkinson P B, 2013. Recent developments in the direct-current geoelectrical imaging method. Journal of Applied Geophysics 95, 135–156.

McPeak S, 2015. Application of the Horizontal to Vertical Spectral Ratio method for delineation of a buried valley near Breckenridge, QC. BSc. thesis, Carleton University, Department of Earth Sciences, Ottawa, Ontario.

McNeely R, Jorgensen P K, 1993. Geological Survey of Canada. Radiocarbon Dates XXXI. Geological Survey of Canada, Paper 91-7, 85 p.

Mangerud J, Bondevik S, Gulliksen S, Hufthammer A, Høisæter T, 2006. Marine $^{14}C$ reservoir ages for 19th century whales and molluscs from the North Atlantic. Quaternary Science Reviews 25: 3228–3245.

Millard A, 2014. Conventions for reporting radiocarbon determinations. Radiocarbon 56(2): 555–559.

Millero FJ, 2013. Chemical Oceanography. 4th Edition, CRC Press, Boca Raton. 591 pp.

Miller R L, Bradford W L, Peters N M, 1988. Specific conductance: theoretical considerations and application to analytical quality control. U.S. Geological Survey Water-Supply Paper 2311, Denver, CO.

Mitchell R J, 1970. Landslides at Breckenridge, Pineview Golf Club, and Rockcliffe, Technical Paper No. 322, Division of Building Research, National Research Council of Canada, Ottawa, June 1970.

Nakamura Y, 1989. A method for dynamic characteristics estimation of subsurface using microtremor on the ground surface; Quarterly Report of Railway Technical Research Institute (RTRI), Japan, v. 30, p. 25–33.

Naldrett D L, 1988. Notes: Sedimentology, stratigraphy and micropaleontology of pre- and early-Champlain Sea fine-grained facies from the Foster Sand Pit, Ottawa, Ontario. Géographie physique et Quaternaire 42(2): 181-189.

Occhietti S, 1976. Dépôts et faits quaternaires du Bas-St-Maurice, Québec (2e partie). Geological Survey of Canada, Paper 76-1C, 3 p.

Occhietti S, Chartier M, Hillaire-Marcel C, Cournoyer M, Cumbaa S L, Harington R, 2001. Paléoenvironnements de la mer de Champlain dans la région de Québec, entre 11 300 et 9750 BP : le site de Saint-Nicolas. Géographie physique et Quaternaire. 55 (1): 23-46.

Oldenborger G A, LeBlanc A-M, 2015. Geophysical characterization of permafrost terrain at Iqaluit International Airport, Nunavut. Journal of Applied Geophysics 123, 36–49. doi:10.1016/j.jappgeo.2015.09.016

Stummer P, Maurer H, Green A G, 2004. Experimental design: Electrical resistivity data sets that provide optimum subsurface information. Geophysics 69, 120–139.

Peacock J D, 1993. Late Quaternary marine mollusca as palaeoenvironmental proxies: A compilation and assessment of basic numerical data for NE Atlantic species found in shallow water. Quaternary Science Reviews 12: 263-275.

Percival J B, Aylsworth A M, Fritz A, 2001. Analysis of colour rhythmites in sensitive marine clays (Leda Clay) from eastern Canada. *In* 2001 A Clay Odyssey; Proceedings of the 12th International Clay Conference, edited by E.A. Dominguez, G.R. Mas and F. Cravero, Bahia Blanca, Argentina, Elsevier, p. 147-154.

Pugin A J-M, Pullan S E, Hunter J A, Oldenborger G A, 2009a. Hydrogeological prospecting using P- and S-wave landstreamer seismic reflection methods, Near Surface Geophysics, 7: 315-327.

Pugin A J-M, Pullan S E, Hunter J A, 2009b, Multicomponent high-resolution seismic reflection profiling, The Leading Edge, 28(10): 1182-1265.

Pugin A J-M, Pullan S E, Hunter J A, 2013a. Shear-wave high-resolution seismic reflection in Ottawa and Quebec City, Canada. The Leading Edge, 32/3, 250-255.

Pugin A J-M, Brewer K, Cartwright T, Pullan S E, Perret D, Crow H, Hunter J A, 2013b. Near surface S-wave seismic reflection profiling– new approaches and insights. First Break 31, 49–60.

Pugin A J-M, Pullan S E, Duchesne M J, 2013c. Regional hydrostratigraphy and insights into fluid flow through a clay aquitard from shallow seismic reflection data The Leading Edge Jul 2013, Vol. 32, No. 7, pp. 742-748. Online Publication Date: July 2013

Reimer P J, Bard E, Bayliss A, Beck J W, Blackwell P G, Bronk Ramsey C, Buck C E, Cheng H, Edwards R L, Friedrich M, Grootes P M, Guilderson T P, Haflidason H, Hajdas I, Hatté C, Heaton T J, Hogg A G,

Hughen K A, Kaiser K F, Kromer B, Manning S W, Niu M, Reimer R W, Richards D A, Scott E M, Southon J R, Turney C S M, van der Plicht J, 2013. IntCal13 and MARINE13 radiocarbon age calibration curves 0-50000 years cal BP. Radiocarbon 55(4): 1869–1887.

Richard P J H, Occhietti S, 2005. $^{14}C$ chronology for ice retreat and inception of Champlain Sea in the St. Lawrence lowlands, Canada. Quaternary Research 63: 353-358.

Rodrigues C G, 1992. Successions of invertebrate microfossils and the late Quaternary deglaciation of the central St. Lawrence lowland, Canada and the United States. Quaternary Science Reviews 11: 503-534.

Rodrigues C G, Richards S H, 1986. An ecostratigraphic study of Late Pleistocene sediments of the western Champlain Sea basin, Ontario and Quebec. Geological Survey of Canada Paper 85-22. 33 p.

SESAME, 2004. Guidelines for the Implementation of the H/V Spectral Ratio Technique Using Ambient Noise Measurements, Processing, and Interpretation, SESAME European Research Project WP12, Deliverable D23.12. ftp://ftp.geo.uib.no/pub/seismo/SOFTWARE/SESAME/USER-GUIDELINES/SESAME-HV-User-Guidelines.pdf [accessed Mar 2017]

St-Jean G, Kieser W E, Crann C A, Murseli S, 2016. Semi-automated equipment for $CO_2$ purification and graphitization at the A.E. Lalonde AMS Laboratory (Ottawa, Canada). Radiocarbon : 1–16. DOI:10.1017/RDC.2016.57

Stuiver M, Polach H A, 1977. Discussion: reporting of $^{14}C$ data. Radiocarbon 19(3):355–63.

Tavenas F, Flon P, Leroueil S, Lebuis J, 1983. Remoulding energy and risk of slide retrogression in sensitive clays. In: Proceedings of the symposium on slopes on soft clays, Linköping, Sweden. Swedish Geotechnical Institute, SGI report no. 17, pp 423–454

Torrance J K, 1976. Pore water extraction and the effect of sample storage on the pore water chemistry of Leda Clay. Soil Specimen Preparation for Laboratory Testing, ASTM STP 599, American Society for Testing and Materials. 147-157

Torrance J K, 1983. Towards a general model of quick clay development. Sedimentology, 30(4): 547-555.

Wasti Y, 1987. Liquid and Plastic Limits as Determined from the Fall Cone and the Casagrande Methods; Geotechnical Testing Journal, GTJODJ, Vol. 10, No. 1, pp. 26-30.

Wilson M E, 1924. Arnprior–Quyon and Maniwaki areas Ontario and Quebec. Geological Survey of Canada, Memoir 136